



Universität Stuttgart

Jahresbericht 2017/2018



Institut für Photovoltaik
Institute for Photovoltaics

Herausgeber

Institut für Photovoltaik
Universität Stuttgart
Pfaffenwaldring 47
70569 Stuttgart

Telefon: +49 711 685 67140
www.ipv.uni-stuttgart.de

Redaktion

J. H. Werner, J. Köhler, J. Nover

Inhaltsverzeichnis

Vorwort Preface	3
1 Arbeitsgruppen Research Groups	6
2 Wissenschaftliche Beiträge Scientific Contributions	16
3 Publikationen Publications	66
4 Was sonst noch war... Beyond Science...	72
5 Lehrveranstaltungen Lectures	76
6 Abschlüsse Degrees	82
7 Mitarbeiter Staff Members	99
8 Lageplan Location Map	105

Institutsleitung und Verwaltung | Head of Institute and Administration

Leitung/Head: Jürgen H. Werner



Liebe Freunde des *ipv/dear friends of the ipv*,
das Institut ist in den letzten zwei Jahren wieder zu einem der stärksten Institute im Fachbereich gewachsen. Die Lehrangebote sind weiter ausgebaut und ergänzt, die Drittmittel für Forschung im Bereich Photovoltaik, Lasertechnik und Energiespeicher gestiegen. Der Umbau des Reinraums und der Aufbau des Labors für Energiespeicher ermöglicht es jetzt, neben den Solarzellen auch an Batteriezellen produktionsorientiert zu forschen. Die Gründung der EnPV GmbH ist ein gutes Beispiel für die Umsetzung von Spitzenforschung in der Photovoltaik in die Produktion umweltfreundlicher und hocheffizienter Module. Aufgrund der Begeisterung unserer Mitarbeiter/innen und Studierenden blicken wir sehr optimistisch in die Zukunft.

During the last two years, the institute became, once again, one of the most prospering institutes in the department. Teaching activities are extended, and third party funds for research in photovoltaics, laser processing and energy storage grew. Even the retrofitting of the clean room – despite many obstacles – is (almost) complete. The new lab for energy storage systems enables us, to work not only on production oriented topics for solar cells but also on batteries. The spin-off EnPV GmbH is a prominent example for the implementation of cutting edge research in the production of environmentally friendly, highly efficient solar modules. In view of the enthusiasm of our employees and students, we are very optimistic about the future of the institute.

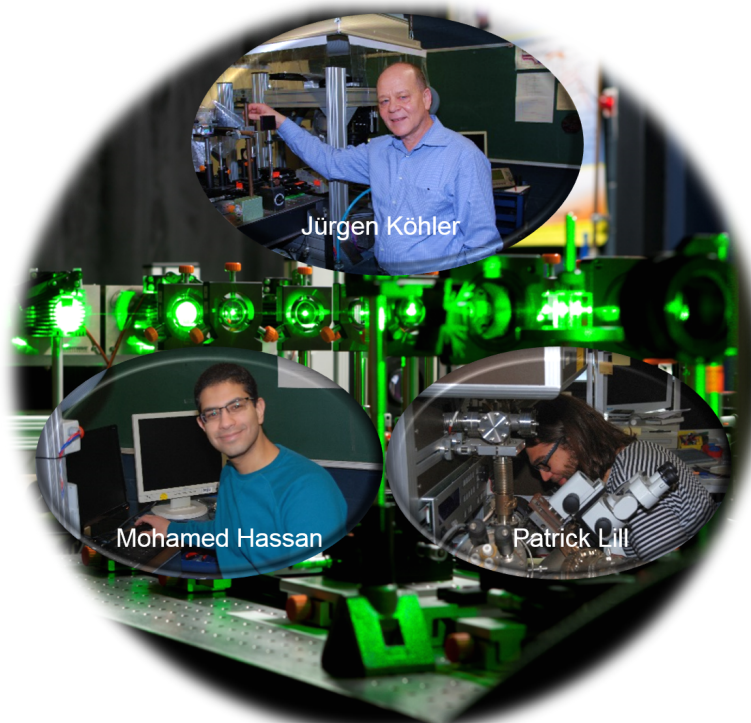
Stuttgart, Dezember/December 2018

Jürgen H. Werner, Markus Schubert, Peter Birke

1 Arbeitsgruppen | Research Groups

Laserprozesse - Laser Processing

Gruppenleiter/Group Leader: Jürgen Köhler



1 Arbeitsgruppen | Research Groups

Die Gruppe „Laserprozesse“ entwickelt neue Technologien zum Laserprozessieren von Materialien für die Elektrotechnik. Neben dem Laser-Prozessieren kristalliner Silizium-Scheiben für Solarzellen und Halbleiterbauelemente, bildet die Herstellung poröser Anoden aus Silizium für Lithium-Ionen Batterien einen weiteren Schwerpunkt. Im Vordergrund unserer Arbeiten stehen die Weiterentwicklung unseres Laserdotier-Prozesses für rückseitenkontakteierte Solarzellen, sowie die Ablation dielektrischer Schichten. Weiterhin untersuchen wir das Dotieren und Aktivieren von Dotieratomen in einkristallinem Germanium für Halbleiterbauelemente sowie das Laser-Porosieren gesputterter Silizium-Schichten. In enger Zusammenarbeit mit den Gruppen „Industrielle Solarzellen“ und „Halbleitertechnologie“ am *ipv* optimieren wir unsere Laserprozesse zur Herstellung hocheffizienter, rückseitenkontakteierter Solarzellen mit Wirkungsgraden über 23%.

The “Laser Processing” group explores new technologies for laser processing of materials for electrical engineering applications. Porous anodes for lithium ion batteries are a new focus of our research, in addition to laser processing of crystalline silicon wafers for solar cells and semiconductor components. The main emphasis of our research lies on pulsed laser doping for high-efficiency back-contact solar cells, and the ablation of dielectric layers. Furthermore, we analyze the doping and dopant-atom activation of mono-crystalline germanium for semiconductor elements, as well as laser porosification of sputtered silicon layers. A close collaboration with the research groups “Industrial Solar Cells” and “Semiconductor Technology” at *ipv* optimizes our laser processes for the fabrication of high-efficiency back-contact solar cells with efficiencies above 23%.

Industrielle Solarzellen - Industrial Solar Cells

Gruppenleiterin/Group Leader: Renate Zapf-Gottwick



Die Gruppe „Industrielle Solarzellen“ forscht und entwickelt an industrienahen Prozessen. Gemeinsam mit den *ipv*-Gruppen „Laserprozesse“ und „Halbleitertechnologie“ arbeiten wir an hocheffizienten Rückseitenkontakt-Solarzellen, die mit Laserprozessen schnell und kostengünstig produziert werden können. In einem vom BMWi und der EnBW finanziertem Projekt verschalten wir diese Zellen zu „grünen“, hocheffizienten Photovoltaik-Modulen, die keine Schadstoffe und keine Edelmetalle enthalten. Zusammen mit einer Firma entwickeln wir für die industrielle Fertigung eine Anlage für die Laserprozesse. In einem weiteren Projekt arbeiten wir an Digitalisierungstechnologien für eine „selbstlernende Photovoltaik-Fabrik“.

Our group “Industrial Solar Cells” is engaged in different research activities for higher efficiencies and less production costs of solar cells in industry oriented processes. Together with the *ipv*-groups “Laser Processing” and “Semiconductor Technology” we develop high-efficient back contact solar cells. The laser processes reduce production cost and process time. In a project, co-financed by BMWi and EnBW, we connect these back contact cells to photovoltaic-modules without using any hazardous materials and noble metals such as silver. In parallel, together with a company we develop an industrially feasible laser-tool. Another project together with four research institutes in Baden-Württemberg has the goal of applying technologies for digitalization for a self-learning photovoltaic-factory – *ipv* working on a digital twin for our laser-tools.

Halbleitertechnologie - Semiconductor Technology

Gruppenleiterin/Group Leader: Birgitt Winter



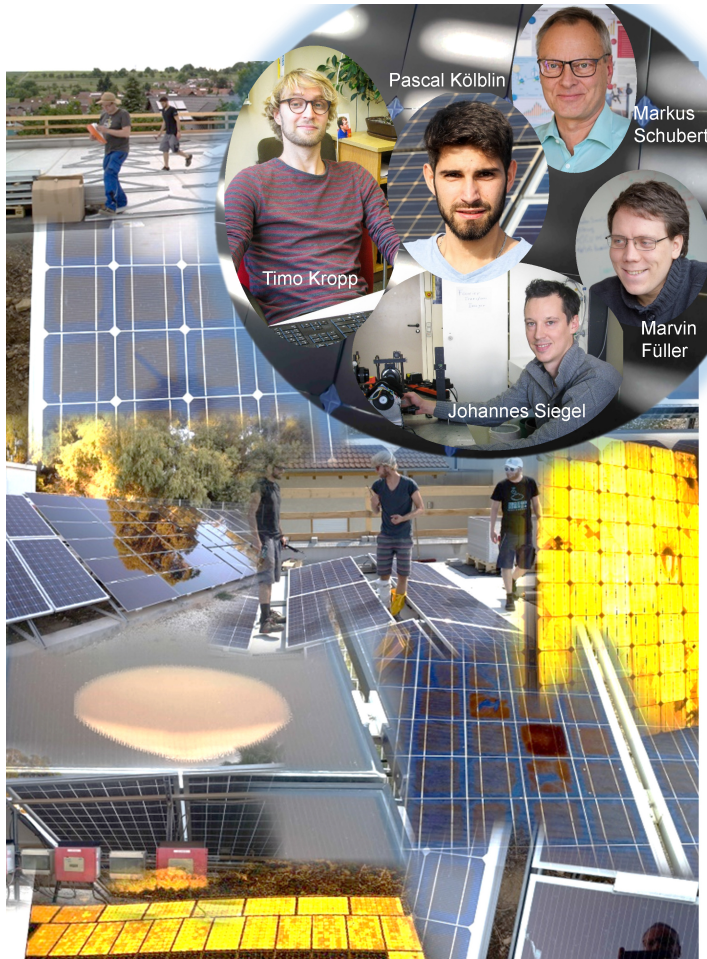
1 Arbeitsgruppen | Research Groups

Die Gruppe „Halbleitertechnologie“ setzt sich aus den technischen Mitarbeiterinnen und Mitarbeitern des gesamten Instituts zusammen. Damit sind verschiedene Aufgabenstellungen zur Absicherung der Institutsinfrastruktur zusammengefasst. Die interdisziplinäre Vernetzung im technischen Bereich ermöglicht eine gute Koordinierung aller anfallenden Arbeiten. Trotz weiterem Umbau des Reinraumlüftungssystems haben wir die routinemäßige Durchführung von Prozessschritten wie Oxidationen, Diffusionen, Plasmadepositionen, nasschemisches Reinigen und Ätzen, Metallisierung, Laserdotieren und vieles andere wiederaufgenommen. Deshalb stand die Anpassung der Prozesse an die Anforderungen zur Prozessierung von hocheffizienten Rückseitenkontakt-Solarzellen im Vordergrund.

The group “Semiconductor Technology” includes all technical assistants and engineers of the institute. By joining forces, we are able to secure the entire infrastructure of the institute. The interdisciplinary composition of the technical team permits optimum coordination of all tasks. Despite further rebuilding of the ventilation system, we have resumed our regular operation of processes, such as oxidation, diffusion, plasma enhanced deposition, wet chemical cleaning and etching, metallization, laser doping, and many others. Therefore, our focus has been led on the adaption of the processes to the requirements of high-efficiency rear-side contact solar cells.

Sensorik - Sensor Technology

Gruppenleiter/Group Leader: Markus Schubert



1 Arbeitsgruppen | Research Groups

Weltweit sind etwa zwei Milliarden Solarmodule in Photovoltaikanlagen installiert. Zur Überwachung der Funktion dieser Anlagen sind effiziente und schnelle Messmethoden erforderlich. Die Arbeitsgruppe „Sensorik“ untersucht in dem vom BMWi geförderten Forschungsprojekt PARK solche Messverfahren, insbesondere auf der Basis von Lumineszenzmessungen bei Tageslicht. Unser Projektpartner Solarzentrum Stuttgart GmbH setzt diese am *ipv* entwickelte Methode weltweit erfolgreich ein. Ergänzend ermöglicht uns die EU COST Action PEARL PV den Austausch mit zahlreichen europäischen Arbeitsgruppen. Innovative bioanalytische Nachweismethoden erprobt unsere Zusammenarbeit mit der Biometrics GmbH, die zusätzlich aus einem Forschungsfonds der Universität Stuttgart unterstützt wird.

Photovoltaic systems contain about two billions of solar modules worldwide. In order to monitor proper function of these photovoltaic systems, efficient and fast diagnostic methods are needed. Our workgroup "Sensor Technology" investigates such methods, in particular based upon daylight luminescence, in the research project PARK. PARK receives funding by the German federal ministry BMWi. Our project partner Solarzentrum Stuttgart GmbH is worldwide sucessfully using daylight luminescence, which was originally developed at *ipv*. The EU COST Action PEARL PV enables exchange on related topics with many workgroups all over Europe. Our co-operation with Biometrics GmbH evaluates innovative diagnostic methods for bioanalytics, funded by a technology transfer fund of the University of Stuttgart.

Elektrische Energiespeichersysteme - Electrical Energy Storage Systems

Gruppenleiter/Group Leader: Peter Birke



Von links nach rechts: Stephan Renninger, Fabian Heim, Sanaz Moameni, Marco Ströbel, Felix Kleinheinz, Alexander Ridder, Peter Birke, Friedrich Speckmann, Jan Singer, Alexander Schmid, Christoph Bolsinger, Daniel Müller.

„Elektrische Energiespeichersysteme (EES)“ umfassen ein sehr weites Feld, denn darunter fallen im Prinzip alle Systeme, die elektrische Energie bidirektional in eine andere Energieform umwandeln können. Die Arbeitsgruppe EES fokussiert sich auf Lithium-basierte galvanische Elemente mit den Schwerpunkten feste Ionenleiter, Phasengrenzen und Strukturierung metallischer Li-Anoden. Systemseitig (Batterie) stehen Energiedichteerhöhung, elektronisches und thermisches Management sowie Batteriemodelle im Vordergrund der Forschung. Der Bereich Power to X (X = gas, liquid, solid), deckt Speicher ab, die als Batterie mit einer einmaligen Aufladung und anschließender Lagerung der Anode verstanden werden können. Die Lagerzeit ist beliebig lange, und die Anode kann danach einfach in einer galvanischen Zelle wieder elektrische Energie liefern.

“Electrical Energy Storage Systems (EES)” cover the wide field of systems that are able to convert electrical energy bidirectionally into another form. The group EES focusses on Lithium-based galvanic elements with research on solid ion conductors, phase boundaries and structures for metallic Li-anodes. On a system level, the focus of research is on energy density enhancement, electrical and thermal battery management and involved battery models. The field of power to X (X = gas, liquid, solid) covers energy systems which can be understood as reserve batteries with a single charge step. The anodes can be separated, stored for an arbitrary time, and reassembled in a galvanic cell to provide energy afterwards.

2 Wissenschaftliche Beiträge |

Scientific Contributions

Identifying Weak Spots in Cadmium Telluride Modules during Long-term Leaching

Jessica Nover

In collaboration with: Renate Zapf-Gottwick, Carolin Feifel, Michael Koch, and Jürgen H. Werner

Leaching of toxic substances out of photovoltaic (PV) modules is of great interest addressed in current research. It is no longer a question if these substances are released in the environment - because several studies proved they do - mostly depending on pH and redox conditions.¹ Today, the questions are: *How* are these substances released? *What* are the weak spots in the modules? *Which* module constituents are responsible for delamination? For this purpose, we analyze not only eluted amounts of toxic substances like cadmium (Cd) from CdTe modules, but also other elements present in the module layers such as tellurium (Te), and molybdenum (Mo) during long-term leaching tests. Module pieces with a size of 5x5 cm² are cut out of commercially available photovoltaic modules and leached in water-based solutions with different pH values to cover a wide range of pH, which can occur in the environment. The

¹A. Ramos-Ruiz et al., "Leaching of cadmium and tellurium from cadmium telluride (CdTe) thin-film solar panels under simulated landfill conditions", Journal of hazardous materials **336**, 57–64 (2017).

experimental method was described elsewhere in greater detail.² Figure 2.1a shows a common structure of a CdTe module with SnO₂ front contact, CdS buffer layer, followed by the CdTe layer and Mo as a back contact. As an example, Fig. 2.1b presents leaching results for this type of module in water-based solutions with pH3. For CdTe module pieces, not only the absorber layer CdTe itself but also the back contact Mo is identified as a weak spot, resulting in high leaching of Cd, Te and Mo. After 1.5 years, we find almost 100 % of the originally contained Cd, Te and Mo in the acidic solution.

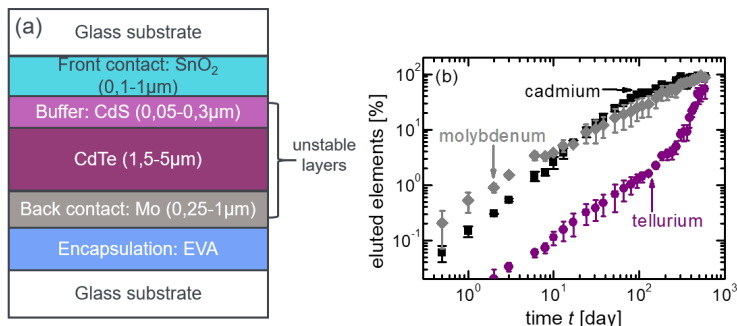


Figure 2.1: a) Typical structure of a CdTe module (not drawn to scale) with the unstable layers CdTe and Mo back contact and b) leaching results of the elements Cd, Te and Mo out of CdTe module pieces in aqueous solutions with pH3.

Long-term leaching tests identify weak spots and unstable layers of PV modules. For CdTe module pieces, we measure high amounts of Cd, Te and Mo in the acidic leaching solutions. Therefore, the module layers themselves are identified being unstable against aqueous solutions.

² J. Nover et al., "Long-term leaching of photovoltaic modules," Japanese Journal of Applied Physics **56**, 08MD02 (2017).

Capacitive Effects in Li-Ion Cells

Alexander Uwe Schmid

In collaboration with: Lukas Lindel and Kai Peter Birke

Each Li-ion cell has a superposed electrostatic double-layer (DL) capacitance caused by the dissociated conductive salt in the electrolyte and the polarized electrodes. Since carbon black is commonly used to improve electronic conductivity of electrodes,³ the question about the size of the superposed DL capacitance arises.

We use electrochemical impedance spectroscopy (EIS) to analyze a Li-ion coin cell with a diameter of $d = 18\text{ mm}$. Its cathode consists of Li-nickel-manganese-cobalt-oxide and the anode is made of graphite. Figure 2.2 presents the capacitance $C_{Xc} = 1/(2\pi f Z'')$ of the Li-ion cell measured by EIS. Here, Z'' is the imaginary part of the cell impedance. It is visible that the capacitance depends on the SOC at frequencies $f < 50\text{ Hz}$. In contrast, the capacitance is independent of the SOC for frequencies $f > 50\text{ Hz}$. This independency is an indicator for the DL capacitance since the frequency is too high for slow SOC-dependent processes like solid particle diffusion or adsorption.

We even distinguish between two other types of capacitance, both depending on frequency:⁴ i) Intercalation capacitance which depends at lowest frequencies $f < 0.3\text{ Hz}$ on the free lattice sites of

³W. Bauer & D. Nötzel, "Rheological properties and stability of NMP based cathode slurries for lithium ion batteries", Ceram. Int. **40**, 4591–4598 (2014).

⁴A. U. Schmid et al., "Capacitive effects in $\text{Li}_{1-x}\text{Ni}_{0.3}\text{Co}_{0.3}\text{Mn}_{0.3}\text{O}_2\text{-LixCy}$ Li-ion cells", J. Energy Storage **18**, 72 –83 (2018).

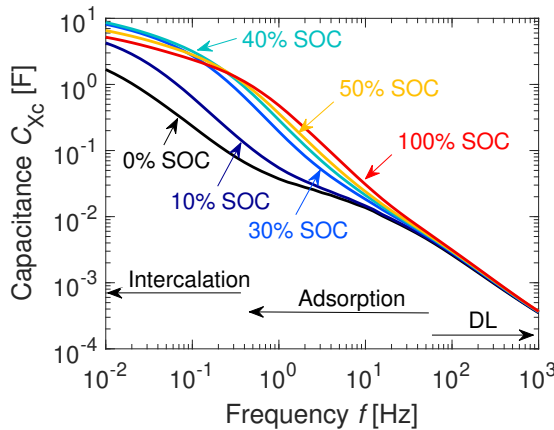


Figure 2.2: Separation of the measured capacitances into three characteristic frequency ranges. Attribution of these ranges to energy storage processes: a) DL capacitance for $f > 50$ Hz, b) adsorption capacitance in the range $0.3\text{Hz} \leq f \leq 50$ Hz, and c) intercalation capacitance for $f < 0.3$ Hz.

the host material. This is the reason why the cell capacitance at 40 % SOC is highest at low frequencies in figure 2.2. ii) Capacitance which is mainly affected by cell voltage at frequencies $0.3\text{Hz} \leq f \leq 50$ Hz probably caused by adsorption.

Power converters, for example in hybrid-electric buses, cause AC harmonics on the DC side at the battery system. Aging experiments of Li-ion cells, applying those AC harmonics on the Li-ion cells, showed that the cells are robust against high-frequent currents.⁵ An explanation is the superposed DL capacitance of the cells.

⁵A. Bessmann, *Interactions between battery and power electronics in an electric vehicle drivetrain* (KTH. Department of Chemical Engineering, SE-100 44 Stockholm, Sweden, 2018).

Laser-IBC Solar Cells with Two Layer Metallization

Renate Zapf-Gottwick

In collaboration with: Erik Hoffmann, Samer Mourad, and Jürgen H. Werner

The Institute of Photovoltaics (*ipv*) develops interdigitated back contact (IBC) solar cells with laser processes yielding an efficiency $\eta = 23.2\%$ on an area $2 \times 2 \text{ cm}^2$ and $\eta = 22.0\%$ on $12.5 \times 12.5 \text{ cm}^2$.^{6,7} By using four laser irradiation steps, the fabrication process avoids any photolithographic masking steps. The laser *dopes* the areas for the pn-junction and the base contact, locally *ablates* a passivation layer for contact formation, and, finally, *structures* the metallization. For an industrial feasible process, we upscale the size of the cells to $15.6 \times 15.6 \text{ cm}^2$ pseudo square wafers. The upscaling requires not only a homogenous doping and deposition of thin layers but also several busbars (BB) on the rear side of the cell. Unfortunately, the BBs with the same polarity as the silicon base material (e.g. negative BB on n-type wafers) cause electrical shading, as the missing pn-junction reduces the carrier collection. A second metallization layer, forming the BBs, avoids this electrical shading and reduces the internal resistance. As a proof-of-concept Fig.2.3a shows a picture of

⁶M Dahlinger et al., "23.2% efficiency with laser processed IBC solar cells", Proc. 31th Europ. Photovolt. Solar Energy Conf, 462–465 (2015).

⁷E Hoffmann et al., "5" Laser-IBC solar cells with 22.0% efficiency", Proc. 32th Europ. Photovolt. Solar Energy Conf, 580–582 (2016).

a “half-cell” cut out of a solar cell with a 156.8 mm edge length. A laser welds and connects six stripes of Al-foil to the contact fingers with the same polarity creating three positive and three negative BBs. Figure 2.3b compares the current density/voltage characteristics of the half-cell with cells on an area of $2 \times 2 \text{ cm}^2$ which are processed in parallel with the BBs aside. The open circuit voltage V_{oc} of the half-cell with an efficiency $\eta_{\text{hc}} = 22.2\%$ is equal to that of the best small cell with $\eta_{2 \times 2 \text{ cm}^2} = 22.6\%$, indicating a laser welding without defects. The worst small cell with $\eta_{2 \times 2 \text{ cm}^2} = 20.2\%$ shows a lower V_{oc} and about the same short circuit current density.

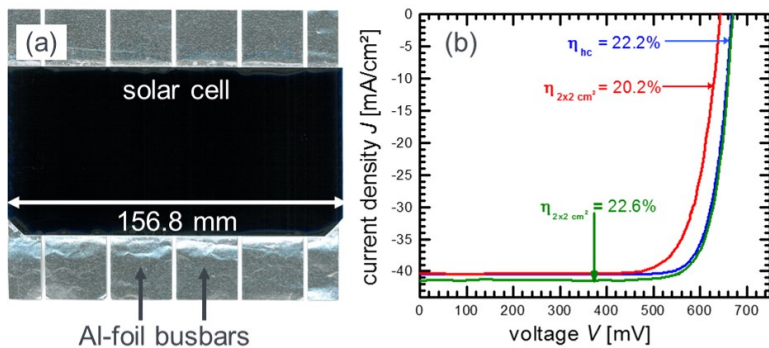


Figure 2.3: a) Picture of the “half cell” cut out of a processed Laser-IBC solar cell with a 156.8 mm edge length. Busbars out of Al-foil are laser welded on the Al-contact fingers. b) Current density/voltage characteristics of the half cell with an efficiency $\eta_{\text{hc}} = 22.2\%$ compared to (in parallel) processed cells on an area of $2 \times 2 \text{ cm}^2$ with the best $\eta_{2 \times 2 \text{ cm}^2} = 22.6\%$ and the lowermost $\eta_{2 \times 2 \text{ cm}^2} = 20.2\%$.

Rectifiers Influence on Efficiency of Alkaline Electrolysis Systems in Dynamic Operation

Friedrich-Wilhelm Speckmann

In collaboration with: Steffen Bintz and Kai Peter Birke

Hydrogen (H_2) has the potential to become a twenty-first century energy carrier. About 95 % of the generated hydrogen is based on fossil fuels, mainly on natural gas.⁸ An environmentally friendly way of hydrogen production is water electrolysis using renewable electrical energy, which can also stabilize the electrical grid. In order to reduce residual load fluctuation, electrolyzers have to be capable of dynamic operation over a wide load range. Experiments show advantages of transistor-based rectifier structures with low current ripples compared to conventional systems in regard to the energy consumption under partial load. Additional measurements identify the negative impact of inadequate rectification on the H_2 gas quality.

A simulation platform is created in order to simulate the output current forms of various rectifier topologies and to downscale these current profiles for testing with a lab-scale alkaline electrolyzer. The variance in the rectification capabilities of the simulated rectifier structures results in additional ohmic losses. While these are negligible for nominal load, their influence increases in partial load. In order to compare the extra energy consumption due to increased

⁸N. Koumi & N. Donatiens, "An overview of hydorgen gas production from solar energy", Renew. Sustain. Energy Rev. **16.9**, 6782–6792 (2012).

current ripples, three conventional rectifiers and a newly designed process current source (PCS) are analyzed. The energy demand of current profiles with load ranges of 25, 50, 75 and 100 % are measured for different topologies. Figure 2.4 shows the consumption of electrical energy for the generation of a fixed amount of hydrogen.

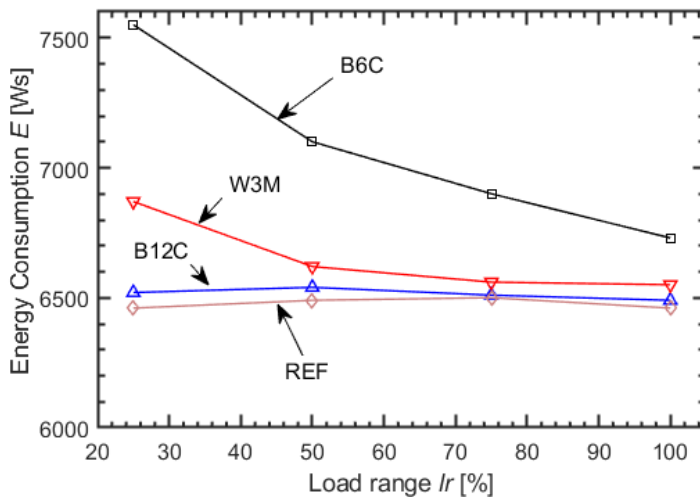


Figure 2.4: Arithmetic mean energy consumption of rectified current profiles from conventional topologies (B6C, W3M, B12C) and PCS (REF).

Topologies that produce high ripple factors, such as six-pulse bridge (B6C) and B6C with an additional thyristor six-pulse bridge (W3M) show decreased efficiency for low load range. Twelve-pulse bridge (B12C) and the PCS perform better due to lower current ripples.

Lifespan of Lithium-Ion Batteries for Second-Life Applications

Daniel Müller

In collaboration with: Kai Peter Birke

Like many other electrochemical cells, lithium-ion batteries exhibit a reduction in performance during use and storage. This is called ageing. For some applications, e.g. electric vehicles, degradation will ultimately result in the replacement of the battery storage. In certain cases, reutilization in a less demanding and more flexible application like stationary storage systems adds considerable monetary value to disused batteries. In turn, a higher market share of electric transportation by reducing the total costs for the consumer can be the result. However, non-linear ageing behavior and in particular the sudden-death of batteries limits their total lifetime and diminishes the benefit of second-life application. Therefore, it is of importance to have detailed knowledge about the ageing behavior of batteries with different cell parameters and configurations. With a model-based study, we investigate the influence of the anode porosity on the capacity retention and, especially, on the sudden-death effect in relation to the second-life concept. We use a extended variant of a physical-chemical model from Yang et al.⁹, which, in turn, is based on the pseudo two dimensional approach

⁹X.-G. Yang et al., "Modeling of lithium plating induced aging of lithium-ion batteries: transition from linear to nonlinear aging", Journal of Power Sources **360**, 28–40 (2017).

by Newman et al.¹⁰ Figure 2.5 shows the capacity retention for two different anode porosity profiles. For the cell with graded anode porosity, the cycle count until sudden-death is doubled, compared to the conventional design. Even though the prolonged lifetime does not influence the primary application a lot, it enables the second-life concept by increasing the useful lifetime for the second-life application significantly. Further investigations will include variation of cell parameters, different operating conditions and especially alternative charging strategies.

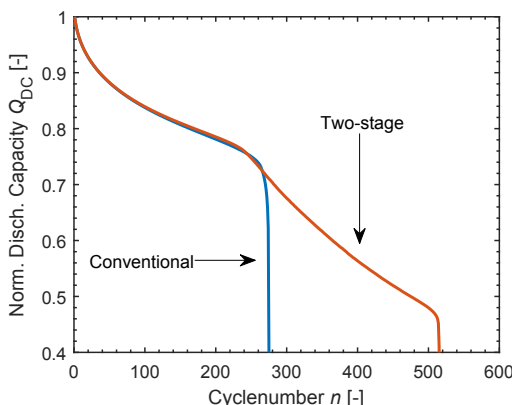


Figure 2.5: Development of discharge capacity during cycling for a conventional anode as well as an anode with two-stage porosity profile. A sudden-death is visible in both cases. Yet the modified porosity profile postpones the sudden-death considerably.

¹⁰M. Doyle et al., "Modeling of galvanostatic charge and discharge of the lithium/polymer/insertion cell", Journal of the Electrochemical Society **140**, 1526–1533 (1993).

Improving Carrier Lifetime in Crystalline n-type Silicon

Samer Mourad

In collaboration with: Renate Zapf-Gottwick and Luis Gottberg

The *ipv*-IBC solar cells achieve high efficiencies $\eta = 23.2\%$ on $2 \times 2 \text{ cm}^2$. Unfortunately, two applied thermal processes degrade the charge carrier lifetime due to the formation of oxide precipitates. Thermal pretreatment to enhance the silicon quality in microelectronics is applied on the used n-type Czochralski (Cz) silicon wafers. Two thermal treatment schemes to dissolve these precipitates were applied, namely, rapid thermal oxidation¹¹ (also named as Tabula Rasa) and “classical” oxidation.¹² Oxide precipitates form due to vacancy-oxygen complexes when the interstitial oxygen atom is mobile at high temperatures. The oxide precipitates undergo two main stages: nucleation and oxide growth. A thermal pre-treatment step grants a dissolution of vacancy oxygen complexes, homogenization of interstitial oxygen distribution in the crystal, and vacancy annihilation. Figure 2.6 shows the photoluminescence (PL) images of monocrystalline n-type semi-square silicon wafers before and af-

¹¹K. Araki et al., “Impact of rapid thermal oxidation at ultrahigh-temperatures on oxygen precipitation behavior in czochralski-silicon crystals”, ECS Journal of Solid State Science and Technology **2**, P66–P70 (2013).

¹²T. Rahman et al., “Minimising bulk lifetime degradation during the processing of interdigitated back contact silicon solar cells”, Progress in Photovoltaics: Research and Applications **26**, 38–47 (2018).

ter thermal processes (phosphorous diffusion plus thermal oxidation) with the corresponding measured initial bulk lifetime τ_{bi} and the final bulk lifetime τ_{bf} . Figures 2.6a and 2.6b show PL images for the reference sample. Without thermal pre-treatment, swirls are formed (oxide precipitate) and the lifetime degrades to $\tau_{bf} = 0.1\text{ ms}$ as shown in fig. 2.6b. Figures 2.6c and 2.6d are the recordings for the sample with Tabula Rasa applied as a pre-treatment. Figures 2.6e and 2.6f are the recordings for the sample with classical oxidation applied as a pre-treatment. Both, the Tabula Rasa and the classical oxidation processes provide homogenization of the luminescence as shown in fig. 2.6d and 2.6f with $\tau_{bf} \geq 1\text{ ms}$.

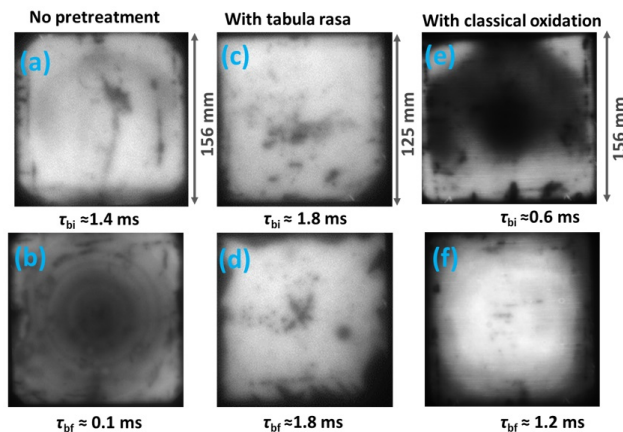


Figure 2.6: Photoluminescence images of monocrystalline n-type semi-square silicon wafers before and after thermal processes with corresponding initial bulk lifetime τ_{bi} and final bulk lifetime τ_{bf} as mean values of nine measurements over the wafer surface. a) and b) correspond to a sample without pretreatment, τ_{bi} degrades from 1.4 ms to $\tau_{bf} = 0.1\text{ ms}$ and swirls occur. c) and d) correspond to a sample with Tabula Rasa, with $\tau_{bi} \approx \tau_{bf} \approx 1.8\text{ ms}$. in e) and f) τ_{bi} is even increased with classical oxidation with $\tau_{bf} \approx 2\tau_{bi}$

Next Generation Lithium-Ion-Cells

Marco Ströbel

In collaboration with: Fabian Heim and Kai Peter Birke

State of the art lithium-ion cells with graphite anodes and liquid electrolyte almost reach the theoretical energy density.¹³ Therefore, the objective of this project is to develop the next generation of lithium-ion accumulators with much higher volumetric energy densities by using lithium-metal anodes and solid state electrolytes (SSE) such as ion-conducting ceramics.

The enhancement of the volumetric energy density is demonstrated in figure 2.7, where a schematic view of a lithium ion cell, an all solid state cell and the striven downsizing of the cell system is shown. Comparing the specific capacity of graphite $C_{\text{graphite}} = 372 \text{ Ah/kg}$ and lithium $C_{\text{lithium}} = 3861 \text{ Ah/kg}$, the specific capacity of the negative electrode is tenfold by using lithium metal.¹⁴

Since there are some challenges by using lithium metal due to the growth of lithium dendrites, it is necessary to replace the conventional separator by a SSE, which is able to transport lithium ions but is stable against dendrites. Until now, there is no procedure to manufacture battery cells with SSE in large quantities. The major key of this project is to develop a SSE system and a fabrication method which is suitable for large scale production. Therefore, the SSE in powder form is combined with additives such as binder and

¹³R. Korthauer, *Handbuch Lithium-Ionen-Batterien* (Springer, 2013).

¹⁴P. Birke & M. Schiemann, *Akkumulatoren: Vergangenheit, Gegenwart und Zukunft elektrochemischer Energiespeicher* (Herbert Utz Verlag, 2013).

lithium-salt to create an ion conducting membrane with separator properties. Currently, different cell designs are under investigation at the *ipv* such as inorganic-, hybrid- and polymer SSE-systems.

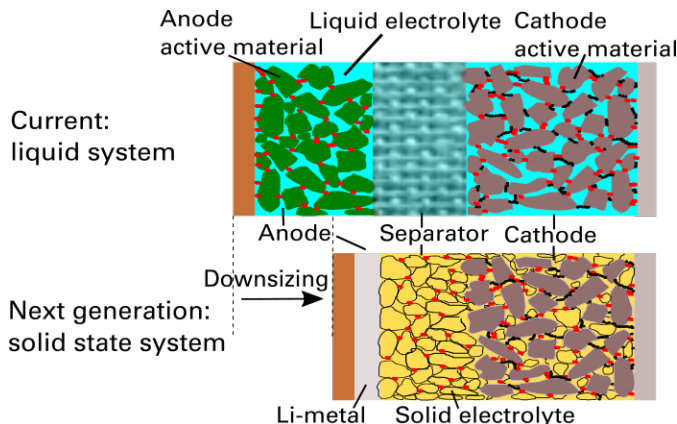


Figure 2.7: Schematic figure of the cell design of lithium ion cells with liquid electrolyte (top) and solid state electrolyte (bottom). There is a high potential to increase the volumetric energy density by downsizing the cell design by using lithium metal electrodes in solid state cells.

From the point of view of electrochemical stability, an all-solid-state system with ion-conducting ceramics is the best solution. Due to the low ionic conductivity at the electrolyte-electrode interface, the SSE-membranes show a specific conductivity of only $\sigma_{\text{SSE}} = 10^{-8} \text{ S/cm}$, instead of the required $\sigma_{\text{req}} = 10^{-4} \text{ S/cm}$. A hybrid system, which combines the stability of the ceramics and the high ionic conductivity of liquid electrolytes, seems to be the most promising option. The next step at the *ipv* will be to find a combination of materials which is electrochemically compatible to create a hybrid composite electrolyte.

Intermediate Layers Improve Laser Welded Contacts

Renate Zapf-Gottwick

In collaboration with: Ahmed Lachhab, Samer Mourad, Jessica Nover, and Erik Hoffmann

The performance of our large area laser processed interdigitated back contact (IBC) solar cells improves by utilizing a second metallization layer as busbars. The busbars are separated from the active cell area (see contribution “Laser-IBC solar cells with a second layer metallization”). The first metallization layer, on the rear side of the cell, consists of aluminium (Al) fingers, which are linearly arranged. The fingers contact the alternatingly doped regions of the pn-junction and the base contact. The Al-foil stripes, perpendicular to the fingers, form the second metallization layer. A laser welding process connects the foil busbars to the fingers of the same polarity, while a dielectric layer between fingers and foil electrically isolates the busbars from the fingers with opposing polarity. However, with this insulating layer, the mechanical stability of the weld seam between fingers and foil degrades. We test different additional layers with varying thicknesses between the foil and the fingers to improve the mechanical stability. Measurements of the peel-off force F (relative to the reference peel off force without intermediate layer F_{ref}) evaluate the effect of the intermediate layer on the laser welding process. Figure 2.8 shows the relative peel-off force F/F_{ref} of Al-foil to an Al-layer measured in the direction 180° to the foil.

Intermediate silicon dioxide (SiO_2) and zinc (Zn) decrease F , while manganese (Mn) and silicon (Si) layers increase F depending on the thickness of the layer. The peel-off force takes a maximum for a thickness $d_{\text{Mn}} = 0.75 \mu\text{m}$ of the Mn-layer and $d_{\text{Si}} = 0.1 \mu\text{m}$ of the Si-layer.

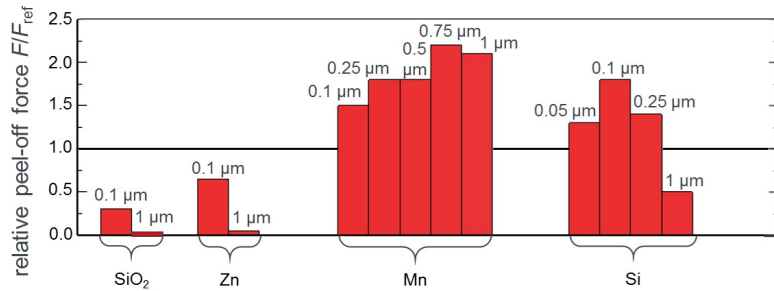


Figure 2.8: Relative peel-off force F/F_{ref} of Al-foil laser welded to evaporated Al with intermediate layers of SiO_2 , Zn, Mn, and Si. Corresponding to the thickness of the different intermediate layers the F/F_{ref} is given. The reference F/F_{ref} represents the peel-off force of Al-foil laser welded to Al without intermediate layer. Layers out of SiO_2 and Zn decrease F , while Mn and Si increase F .

Thermal Gradients inside Cylindrical Battery Cells

Christoph Bolsinger

Due to the different layers of the electrodes, lithium-ion cells show highly anisotropic thermal properties. This leads to high thermal gradients and a non-uniform temperature distribution inside the cell which affects the local current densities as well as the local charge carrier distribution. These inhomogeneities lead to reduced performance, local aging differences inside the cell and an accelerated global cell aging process.¹⁵ Thermal management systems prevent these inhomogeneities by reducing the thermal gradients inside the cells with an optimal cooling configuration. Therefore, we investigate the effect of a terminal and a surface cooling configuration on the thermal gradients inside a cylindrical 26650 LiFePO₄/graphite cell. The terminal cooling configuration dissipates the heat from the cells terminals, whereas the surface cooling configuration cools the cell housing.

Three integrated NTC thermistors measure the core temperature at different locations and enable the determination of the thermal gradients during the operation. Figure 2.9 (a) shows the locations of the core temperature T_c and the surface temperature T_s measurements

¹⁵M. Fleckenstein et al., "Current density and state of charge inhomogeneities in li-ion battery cells with LiFePO₄ as cathode material due to temperature gradients", Journal of Power Sources **196**, 4769–4778 (2011).

with their corresponding abbreviations. Alternating current pulses heat up the cell without varying the average state of charge and, therefore, enable the operation in the thermal steady state for different investigated cooling capacities. Calculation of the generated heat flow and the cooling capacity allows the comparison of the thermal gradients between both cooling configurations.

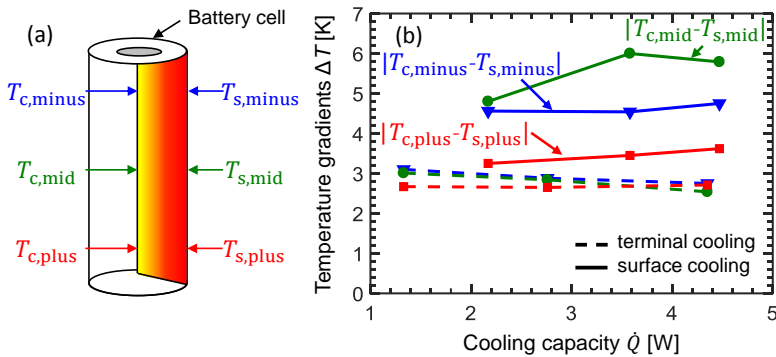


Figure 2.9: (a) Location of the temperature measurements with the respective abbreviations. (b) Thermal gradients inside the cells at three different axial positions for different cooling capacities.

Figure 2.9 (b) shows the radial temperature gradients for the terminal and the surface cooling configuration in relation to the respective cooling capacity. The thermal gradients inside the cell in the terminal cooling configuration are decreased up to a factor of two compared to the thermal gradients inside the cell in the surface cooling configuration. Therefore, the terminal cooling configuration cools the cell more uniformly which probably results in a slower aging process compared to the surface cooling configuration.

Finger Interruptions in Screen-printed Solar Cells

Matteo Schiliró

In collaboration with: Renate Zapf-Gottwick

The application of the metal contacts is one of the last steps in the production of solar cells. If the contacts have interruptions, we expect losses in the performance of solar cells.¹⁶ The goal of our work is to create and investigate solar cells with defined interruptions in the silver contact fingers on the front side of the solar cell. The experiments allow us to determine and to understand the impact of these defects on the cell performances, such as the efficiency η and the fill factor FF . The interruptions are classified according to their size S , number n and distance to the busbar x_F . The defects on the cells are generated by screen printing. In order to obtain reproducible, defined and precise interruptions in dimension and position, a special screen filler fills the openings of the screen. Experiments with different targeted screen printed finger interruptions are carried out.

Figure 2.10a shows a photograph of a part of the cell's front side with defined finger interruptions. Figure 2.10b illustrates the effect of the finger interruptions on the efficiency of the solar cells. An efficiency loss $\Delta\eta_{abs} > -0.15\%$ needs a number $n \geq 60$ of finger interruptions and for an $\Delta\eta_{abs} \approx -0.4\%$ a $n = 102$, for $S \geq 500\text{ }\mu\text{m}$. A

¹⁶R. De Rose et al., "A methodology to account for the finger interruptions in solar cell performance", *Microelectronics Reliability* **52**, 2500–2503 (2012).

smaller $S_1 = 300 \mu\text{m}$, results in $\Delta\eta_{\text{abs}} \approx -0.25\%$ with $n = 102$ interruptions, corresponding to the total number of fingers. An increased series resistance mainly causes the lower FF and the lower efficiency. The short circuit current and the open circuit voltage remain almost constant.

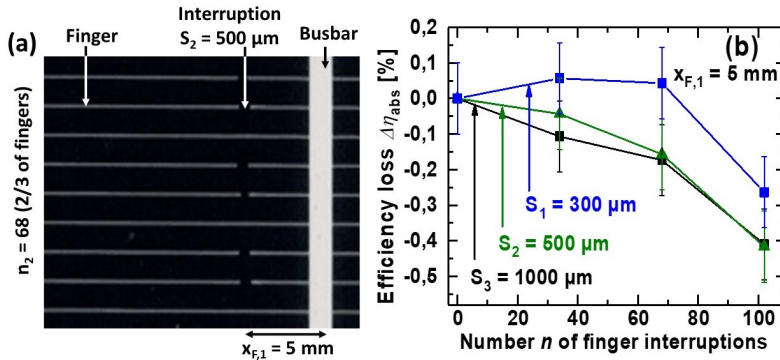


Figure 2.10: a) Details of the front side of a solar cell with $n = 68$ finger interruptions (2/3 of the fingers) of $S = 500 \mu\text{m}$ and $x_{F,1} = 5 \text{ mm}$ away from the busbar. b) Efficiency loss $\Delta\eta_{\text{abs}}$ of the solar cells with different number ($n_1 = 34$, $n_2 = 68$, $n_3 = 102$) and different sizes ($S_1 = 300 \mu\text{m}$, $S_2 = 500 \mu\text{m}$ and $S_3 = 1000 \mu\text{m}$) of finger interruptions at a distance of $x_{F,1} = 5 \text{ mm}$ from the busbar.

The experiments show which size, number and position of the finger interruptions lead to losses of efficiency. Finger interruptions with $S \geq 500 \mu\text{m}$ cause noteworthy $\Delta\eta_{\text{abs}} > -0.2\%$. For $n \geq 60$, a vision system as a process control for screen printing detects finger interruptions in sizes of $20 \mu\text{m}$. As a consequence, a vision system enables a so-called “digital shadow” to recognize and act for correcting the defects.

Challenges during Electrode Preparation for Lithium Ion Cells

Alexander Ridder

In collaboration with: S. Lukas, C. Lieber, K. P. Birke

The two main electrodes used for lithium ion cells are graphite and lithium nickel cobalt manganese oxide (NCM). Finding the right parameters for the preparation of those, is a huge effort as not only composition and thickness of the electrode, but also things like mixing time and drying procedure must be considered.

We produce electrodes by mixing active material (Graphite/NCM), conductive additive and binder in solution. We mingle the slurry in a planetary mixer, which can be used as a planetary mill to reduce agglomerates.

By the application of a doctor blade for the production of homogeneous films, we coat the slurry on a current collector. Drying is done at 120 °C, first in ambient atmosphere and afterwards under vacuum. In a glove box we build the electrodes in coin cells against lithium metal to test their cyclic stability.

Figure 2.11 shows the capacity and Coulombic efficiency versus cycles of one of the built cells, which consists of a NCM-111 electrode, a lithium metal counter electrode and a Polypropylene separator with 1 M LiPF₆ in Ethylenecarbonato:Diethylenecarbonate (1:1) electrolyte. It can be seen that the cell provides 80 percent of its original capacity after 66 cycles at a discharge rate of 1C.

Different sorts of graphite, electrode composition, mixing with and

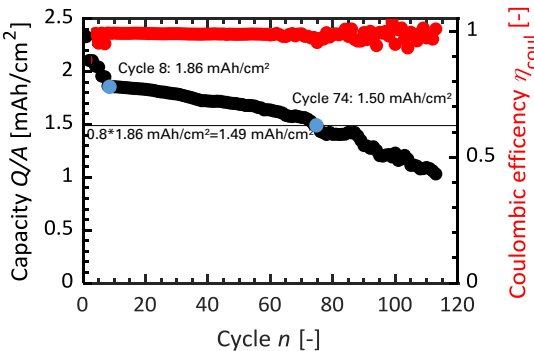


Figure 2.11: Capacity and Coulombic efficiency over cycles for an NCM-111 electrode vs lithium with LiPF_6 electrolyte.

without use of an ultrasonic bath, as well as varied drying procedures and thickness of electrodes were investigated. We produce graphite electrodes without conductive additive, as graphite possesses sufficient electrical conductivity. The significance of the temperature profile during the drying process is still investigated. The usage of styrene-butadien-rubber/carboxy-methyl-cellulose binder instead of Polyvinylideneflouride seems to increase the cycle stability, while the usage of a primer for a better adhesion on the current collector seems to be unnecessary.

We show that the production of stable electrodes with a decent capacity is influenced by many factors and needs further investigation. The electrodes are the basis for pouch cells that are build for the investigation by computed tomography to better understand aging phenomena. Additionally we generate data for the development of a model for the prediction of aging with partners from Berlin, Ulm and Münster.

Laser Doping for Crystalline Silicon Solar Cells

Mohamed Hassan

In collaboration with: Jürgen R. Köhler and
Jürgen H. Werner

Laser doping delivers the high spatial resolution which is required for interdigitated back contact solar cells, without any masking processes.^{17,18} On p-type silicon wafers, laser doping provides the boron atoms for the n-type emitter. The source for boron is a sputtered boron oxide precursor. This work studies the influence of the pulse to pulse distance O_x on the resulting sheet conductance G of the doped area. Our experiments demonstrate that a decreased pulse to pulse distance O_x decreases the required pulse energy density H to form continuously electrically connected doped regions. A decreased pulse to pulse distance O_x leads to increased re-condensation of boron on the surface, resulting in a higher sheet conductance G . Figure 2.12 shows the influence of pulse to pulse distance O_x on the sheet conductance G . The width w of the line focused laser beam is $w = 19 \mu\text{m}$. Increasing the pulse to pulse distance O_x between subsequent laser pulses increases the threshold pulse energy density H_{th} . The formation of continuously doped areas requires more pulse energy when the distance between subsequent pulses O_x increases. The maximum reachable sheet

¹⁷T. Röder et al., “Add-on laser tailored selective emitter solar cells,” Progress in Photovoltaics: Research and Applications **18**, 505–510 (2010).

¹⁸M. Dahlinger et al., “Full area laser doped boron emitter silicon solar cells,” in (PVSC, IEEE, 2012), S. 001029–001031.

conductance G_{\max} increases with decreasing the pulse to pulse distance O_x . The amount of re-condensed boron increases when the individual laser pulses move closer together. When the pulse energy density reaches a certain value H_{drop} the sheet conductance decreases. A possible, not yet proven, cause is, that the evaporation of the precursor layer exceeds the amount of boron re-condensation. The constant sheet conductance G for $H > 2.4 \text{ J/cm}^2$ for the smallest pulse to pulse distance $O_x = 1.8 \mu\text{m}$ is presumably due to the balance between precursor evaporation and re-condensation of the evaporated material.

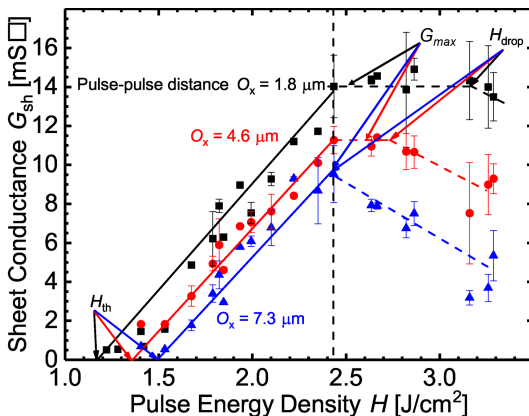


Figure 2.12: The sheet conductance G increases with decreasing the pulse to pulse distance O_x of a line-focused pulsed laser beam. A larger pulse to pulse distance O_x leads to a higher threshold pulse energy density H_{th} , because electrically connected areas require more pulse energy when O_x increases. The maximum reachable sheet conductance G_{\max} increases with decreasing O_x due to increased boron re-condensation by closer pulses. The decrease of the sheet conductance for higher pulse energy densities presumably results from increased evaporation of the precursor layer at high pulse energy densities.

Temperature Estimation with Artificial Neural Network

Felix Kleinheinz

In collaboration with: Christopher Schuchert and Kai Peter Birke

Temperature estimation for Lithium-Ion-Cells is crucial for modern Battery-Management-Systems to detect failures and ageing. The present study investigates a new sensorless method to determine the cell temperature. The method is based on electrochemical impedance spectra for a 18650 lithium-iron-phosphate cell under load. It replaces single-frequency methods in literature by training an Artificial Neural Network (ANN) with all frequency data.¹⁹ Further, the ANN handles cell-to-cell variances. Figure 2.13 shows the temperature and cell variance influence on the impedance spectra. Different manufacturing parameters, storage periods or transport conditions impair the specific cell's impedance spectra. Experimental investigation at nine 18650 cells show a variance for the inner resistance up to 10 %. A multi-cell-holder for up to nine 18650 cylindrical cells was constructed to generate reproducible impedance measurement data between 10 Hz and 10 kHz. At temperatures above 0 °C, the chosen frequency range is independent of overlaying direct cell current. The method works with measurements of an impedance

¹⁹J. P. Schmidt et al., "Measurement of the internal cell temperature via impedance: Evaluation and application of a new method," Journal of Power Sources **243**, 110–117 (2013).

spectra under load or directly after interrupting load. The trained network shows best performance with six hidden neurons while using real and imaginary data as model input. Estimation accuracy without load is 2 K and with load 7 K.

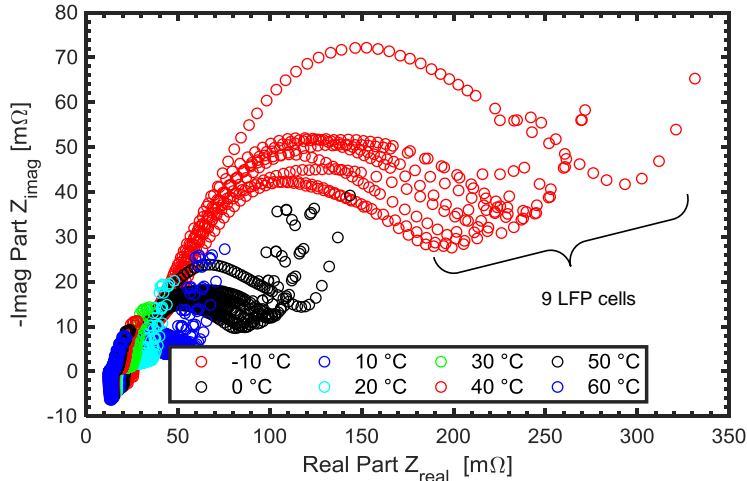


Figure 2.13: Impedance spectra for identical nine 18650 Lithium-Ion cells with $I = 100\text{ mA}$ in a temperature range between -10°C and $+60^\circ\text{C}$. Frequency sweeps between 10 mHz and 10 kHz with no overlaying DC. Internal resistance decreases with higher temperatures which is related to the electrochemical process inside the cell. Data set is used to train a Neural Network for temperature estimating. Cell variance deteriorated the estimation performance.

Next to the inner temperature, further work investigates the possibility to estimate additional states like State of Charge or State of Health. To measure frequency based impedance values, a special measurement equipment is necessary. A recurrent ANN for time dependent data get around this problem.

Machine learning for defect detection and classification in electroluminescence images

Pascal Kölblin

**In collaboration with: Qiang Chen, Alexander Bartler,
Solarzentrum Stuttgart GmbH**

Electroluminescence (EL) is an image-based measurement technique to identify various defect types in solar cells. We show how defects are detected, located, and classified from EL images by an artificial neural network (ANN). Automated defect detection and classification is important for analyzing large numbers of EL images according to the influence of defects and risk classification of cells and modules. Common approaches in literature²⁰ classify defective solar cell areas in three categories with respect to their effect on the electrical performance:

type A - no influence on power production

type B - defective areas with decreased power production

type C - defective areas with (almost) no power production

Figures 2.14c and 2.14d present results of the automated defect detection in an EL image of a solar cell by an ANN. Here adequate pre-processing of the EL images is crucial for reliable results, i.e. correction of lens and camera errors, cell finding within the module etc.

²⁰DIN IEC/TS 60904-13:2016-10, *Photovoltaic devices - Part 13: Electroluminescence of photovoltaic modules (IEC 82/1062/CD:2016-10)(VDE V 0126-4-13:2016-10)*, Norm, Berlin, 2016.

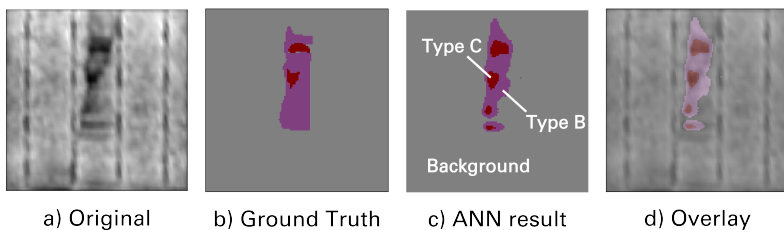


Figure 2.14: a) Original greyscale EL image. b) Ground Truth labeled image (defects marked by an expert). c) Defects recognized and marked by the ANN. d) Overlay of original a) and ANN classification c).

The EL greyscale image Fig. 2.14a presents type C defects in black, whereas type B defects appear dark but not completely black. The result of automated classification by ANN in Fig. 2.14c marks type B and type C defects in front of the background, which also includes type A classified defects. Training of the ANN by datasets similar to Fig. 2.14b that were labeled by human experts, enables defect classification with a pixel accuracy of 89 % for type C and 47 % for type B. Nevertheless, a global pixel accuracy of 98 % shows, that a high accuracy in differentiating between the defect types is achieved, even if the background is inhomogeneous. For further quantification, defect areas and locations are identified and a map of defect coordinates exported. Future work strives to improve the precision of the detection by ANN processing, and yields input datasets for analyzing the electrical output of solar cells and modules with defects.

Lithium Metal Electrodes for Rechargeable Batteries

Fabian Heim

In collaboration with: Tina Kreher and Kai Peter Birke

The current technology of lithium-ion cells is about to reach its limits considering energy density. Lithium metal electrodes have the potential for further optimization but bring along several challenges that need to be overcome. Lithium, like most metals, deposits forming dendritic structures with large surface area. Those structures may lead to cell short-circuit by piercing through the separator. Another issue is the consumption of active lithium and components of the liquid electrolyte due to inefficient passivation. The formation of dendritic structures is amplified by inhomogeneous current density induced by natural protrusions on the electrode surface and inhomogeneities in the thickness of the passivating layer.²¹ One solution for reducing locally increased current densities is by creating an electrode with a large surface area. Another approach is the optimization of the electrolyte to improve the properties of the passivation layer on the lithium metal electrode. We investigate mechanically and chemically manufactured metal structures as hosts for lithium metal electrodes including ones. The experiments show that mechanical methods like weaving of metal wires or slitting and stretching of metal foil are not suited for generating sufficiently fine

²¹Q. Li et al., "3D Porous Cu Current Collector/Li-Metal Composite Anode for Stable Lithium-Metal Batteries", Advanced Functional Materials **27**, 1606422 (2017).

structures. Chemical etching of metal alloys like bronze and brass or electrochemical deposition of dendritic copper onto metal foil however generate porous structures which provide a high surface area. Figure 2.15 displays a comparison of the plating and stripping behavior of lithium onto different metal structures using a typical liquid electrolyte for lithium-ion cells. The repeatability of the reaction, depicted as the reached number of cycles of the plating and stripping of lithium, is displayed against the reversibility of the reaction depicted as mean Coulombic efficiency.

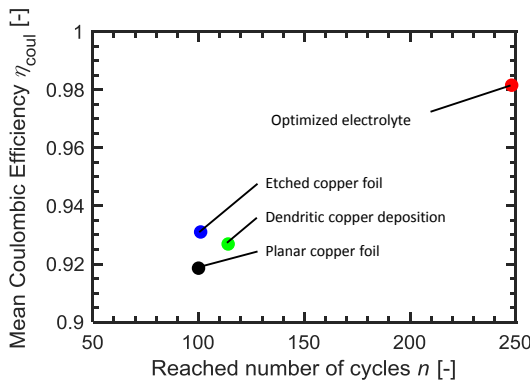


Figure 2.15: Comparison of different cycling experiments with lithium metal electrodes. Changing the electrolyte composition has a much greater influence on the cycle behavior of lithium metal electrodes than improving the electrodes surface structure.

Our results indicate a slight improvement of structured metals compared to planar foil especially considering Coulombic efficiency. Whereas replacing the electrolyte by one forming a more efficient passivation layer has a much greater effect in terms of both maximum number of cycles and efficiency.

Surface Patterning of Monocrystalline Silicon Induced by Spot Laser Melting

Tobias Menold

**In collaboration with: Mawuli Ametowobla,
Jürgen R. Köhler, Jürgen H. Werner**

Surface patterning of silicon recently has become interesting for applications in the fields of microelectronics and micromechanics. Unfortunately classical patterning techniques such as photolithography is tedious and requires complex sample preparation.

In order to overcome this problem, we produce defect free surface patterns with the help of a low cost microsecond laser, that are characterized by a central peak structure and quasi-periodic ripples.

Figure 2.16 (a) shows an example structure, created by a $\tau_p = 85 \mu\text{s}$ long laser pulse with $E_p = 5.5 \text{ mJ}$ pulse energy.

The central peak forms due to silicon's anomalous mass density. When silicon solidifies, it needs approximately 10% more volume. Thus, solidifying and expanding material forces the remaining liquid material to rise. Figure 2.16 (c) shows, that the choice of laser pulse energy E_p exactly controls the peak height z_{\max} .

The quasi-periodic ripples stems from a standing capillary wave, that is excited in the melt pool due to thermocapillary convection.²² A new analytical fluid dynamic model for the capillary wave enables us to calculate the radius of the jth ripple. Figure 2.16 (b) com-

²²T. Menold et al., "Surface patterning of monocrystalline silicon induced by spot laser melting", Journal of Applied Physics **124**, 163104 (2018).

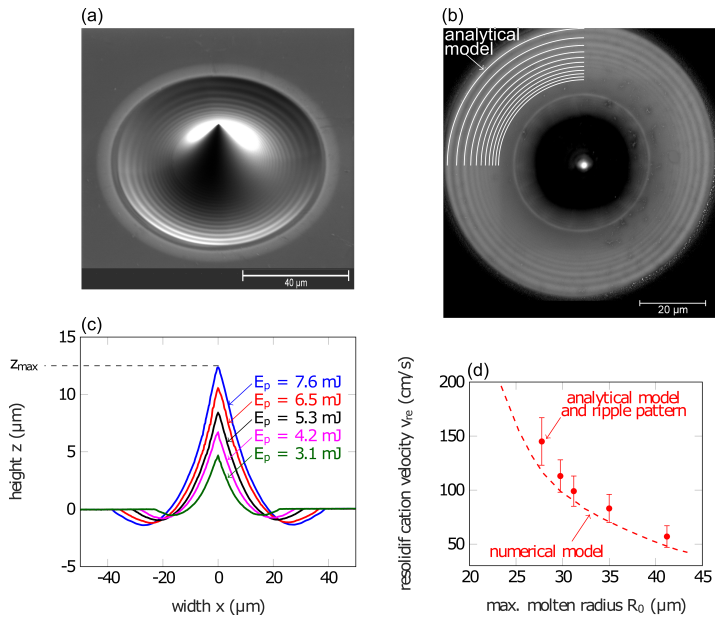


Figure 2.16: Spot laser melting of monocrystalline silicon induces a characteristic surface structure after resolidification. The scanning electron microscope (SEM) images in (a) and (b) and the topographies in (c) show a central peak and quasi-periodic ripples. A new analytical model explains the peak, as well as the ripples and enables us to calculate the resolidification velocity from the ripple pattern (d).

pares the ripple radii determined by our analytical model with the structure of Fig. 2.16 (a) shown from top view.

Additionally, the analytical model predicts the resolidification velocity v_{re} of laser molten silicon. Figure 2.16 (d) compares resolidification velocities v_{re} determined by our analytical model with one determined by a numerical *ab initio* model for different sized structures.

Solid Polymer Electrolyte for Li-Ion Batteries

Sanaz Momeni

In collaboration with: Kai Peter Birke

Solid Polymer Electrolytes (SPE) for Lithium-ion (li-ion) batteries have been a popular research field since the discovery of ionic conductivity in lithium salt complexes of polymers like Poly(ethylene oxide) (PEO)²³. SPEs are interesting alternatives to liquid electrolytes due to the improved mechanical properties and consequently safer performance for the future li-ion cells. The challenge is to combine high mechanical stability with good ionic conductivity together with electrochemical stability in a single polymer membrane, which is the ultimate goal of this study. According to literature, PEO is one of the most attractive SPEs among other polymer candidates for Li-ion cells due to high solubility for lithium salts²⁴; However, because of its limited electrochemical window using it with high voltage cathodes like NCM (LiNiCoMnO_2) is not possible. In this experimental work, we attempt to improve the electrochemical stability of a PEO-based membrane.

Figure 2.17a shows the cyclic voltammetry (CV) results of three different membranes indicating that blending the PEO polymer with Polymethylmethacrylate (PMMA) extends the working window to the voltages around 4.3 V vs. Li/Li^+ . In contrast, the block copoly-

²³E. Rietman et al., "Alkali metal ion-poly (ethylene oxide) complexes. ii. effect of cation on conductivity", Solid State Ionics **25**, 41–44 (1987).

²⁴Z. Xue et al., "Poly (ethylene oxide)-based electrolytes for lithium-ion batteries", Journal of Materials Chemistry A **3**, 19218–19253 (2015).

mer of Poly (ethylene oxide-*b*-styrene) has the similar stability as the pure PEO.

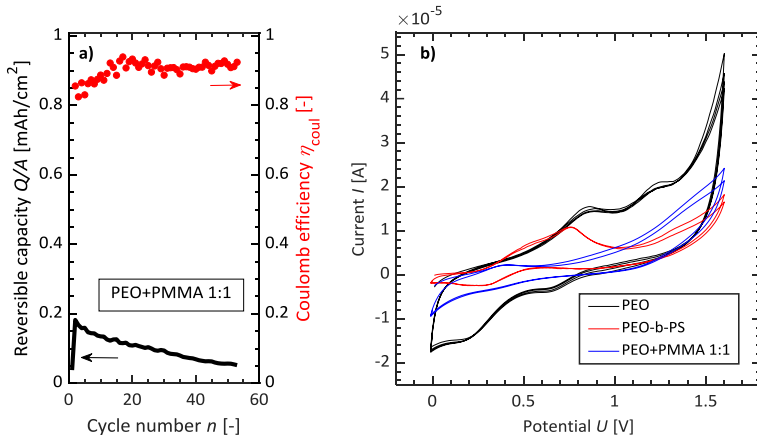


Figure 2.17: a) Discharge Capacity (black) and Coulomb Efficiency (red) vs. cycle number of a coin cell with NCM/PEO+PMMA 1:1/Li components. b) Cyclic Voltammetry of PEO, PEO-*b*-PS and PEO+PMMA 1:1 in the voltage range of 0-1.6 V vs. Ag/AgCl.

A coin cell using NCM cathode, blend of PEO:PMMA (1:1 wt%) as the free-standing solid membrane and Li metal anode is assembled and tested for over 50 cycles. Figure 2.17b) depicts the cycling results. Although the cell shows capacity fading the Coulomb efficiency is around 0.9 and the cell works stable.

In future, we aim to optimise the electrochemical stability of membrane to reach 5V vs. Li/Li⁺ as well as ionic conductivity to achieve low temperature $T < 40^{\circ}\text{C}$ cycling. For this purpose, the layered membrane of PMMA/PEO and its differences with the blended one is our point of interest for further investigation.

Power Loss Prediction of Damaged Photovoltaic Modules

Timo Kropp

**In collaboration with: Markus Schubert and
Jürgen H. Werner**

Electroluminescence (EL) imaging is one of the most common methods to evaluate the degradation state of a photovoltaic (PV) module. For example, due to their low luminescence intensity, cell cracks as well as partially and fully disconnected cell areas are visible in case of modules built from crystalline silicon. However, a direct quantitative prediction of electrical module performance purely based on EL images has yet to be accomplished. Our novel approach uses just one single EL image to predict the electrical loss of mechanically damaged modules when compared to their original (data sheet) power.²⁵ First, one EL image, taken at current injection of the order of the short circuit current, is converted into a locally resolved (*relative*) series resistance image. From the known, totally injected current to the module, we are then able to calculate the *absolute* series resistance values and the local distribution of voltages and currents. This calculation of the series resistance image is an iterative procedure. By choosing one or multiple cells without defects in the series resistance image as reference, the resistance image gets calibrated. The iterative procedure compares the mean

²⁵T. Kropp et al., "Quantitative prediction of power loss for damaged photovoltaic modules using electroluminescence," Energies **11**, 1172 (2018).

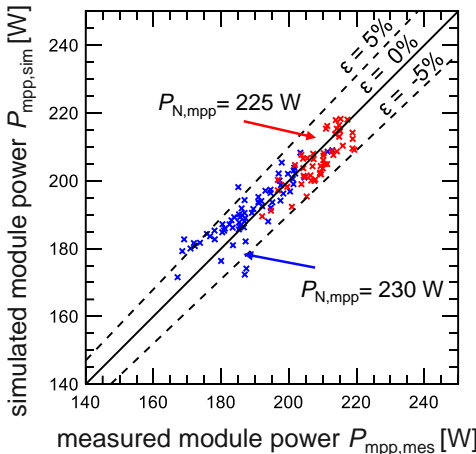


Figure 2.18: Comparison of simulated module power $P_{\text{mpp},\text{sim}}$ and the measured power $P_{\text{mpp},\text{mes}}$ at the maximum power point. The 143 modules are separated into two power categories based on the data sheet power ($P_{N,\text{mpp}} = 225 \text{ W}$ in red crosses and $P_{N,\text{mpp}} = 230 \text{ W}$ in blue crosses).

series resistance of the reference cells to the series resistance of the defect-free original module, derived from its data sheet values. The iteration generates new series resistance images, until the series resistance of the reference cells coincides with the one of the defect-free original module. Based on the calibrated series resistance image, our simulation then predicts the overall current/voltage characteristics of the defective module. We experimentally validate this imaging method and the simulation model via the characterization of 143 PV modules. Each module contains 60 multicrystalline silicon solar cells that were mechanically damaged by hail. Figure 2.18 compares the simulated module power $P_{\text{mpp},\text{sim}}$ to the measured power $P_{\text{mpp},\text{mes}}$ at the maximum power point. Our novel method accurately evaluates most modules (93 %) with a deviation $\epsilon < 5 \%$ between simulated and measured power. The mean deviation $\bar{\epsilon} < 3 \%$ is within the typical uncertainty of data sheet power due to measurement error and sorting tolerances.

Pressure Monitoring Cell for Constrained Battery Electrodes

Jan Singer

In collaboration with: Christian Sämann, Tobias Gössl, and Peter Birke

Constraining battery electrodes extends the cyclic lifetime of the battery cell. Several aging effects like electrode degradation and particle cracking might be reduced by applying a small pressure p on the electrodes surface.²⁶ Further, in the case of Lithium-ion cells, there is a steady growth of surface films like the solid electrolyte interface (SEI). On the one hand, the SEI protects the active material against the electrolyte. On the other hand, a steady growth means a loss of cycling capacity of the cell and an increasing internal cell pressure. The steady SEI growth might be controlled by constraining the electrodes with an optimal cell pressure. To investigate single electrode cells, we developed a pressure monitoring cell, as shown in Fig. 2.19 a).

The pressure monitoring cell allows us to adjust a cell pressure and to monitor the pressure change due to cycling and aging effects of coin cells with a diameter $d = 18\text{ mm}$. New material compositions, preparations methods and testing of new electrolyte additives can be tested by measuring the cell pressure. Fig. 2.19 b) illustrates the functionality of the cell by measuring the voltage V and pressure

²⁶J. Cannarella & C. B. Arnold, "Stress evolution and capacity fade in constrained lithium-ion pouch cells", Journal of Power Sources **245**, 745–751 (2014).

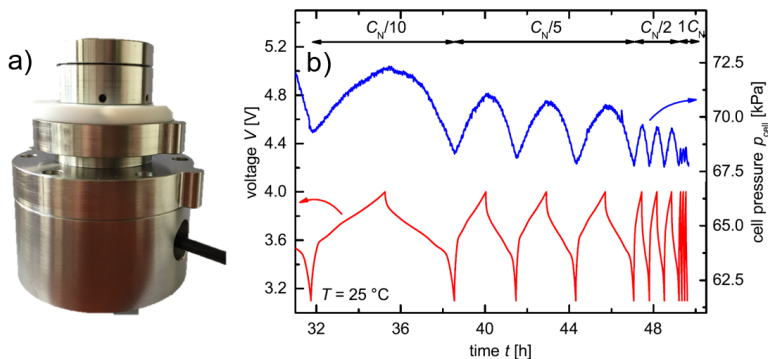


Figure 2.19: a) Pressure monitoring cell. b): C-Rate dependent voltage and pressure curve of constrained NCM/graphite cell set-up demonstrates the functionality of the pressure monitoring cell.

curve p_{cell} of a NCM / graphite cell during cycling using a current of $I = C_N/10, C_N/5, C_N/2$ and $1C_N$. While charging the cell, the negative graphite anode increases its volume up to $\Delta V_A = 10.6\%$ and the positive NCM cathode shrinks down to $\Delta V_K = 2.44\%.$ ²⁷ The resulting volume change of the full cell, consisting of the anode and the cathode, is measured as pressure change Δp . Depending on the C-Rate, the maximum cell pressure decreases with a increasing current due to thermal expansion and missing mechanical relaxation as a consequence of high kinetics. In future work, we will determine the influence of the external cell pressure on the formation of the electrodes surface layers. Further, the optimum pressure for different electrode materials will be targeted to reach a maximum cycling lifetime.

²⁷W. H. Woodford et al., "Design criteria for electrochemical shock resistant battery electrodes", Energy & Environmental Science **5**, 8014 (2012).

Segregation of Boron and Antimony in Liquid Silicon

Patrick Lill

In collaboration with: Morris Dahlinger and
Jürgen R. Köhler

Melting silicon locally with a pulsed laser is an established method to enable diffusion of dopants which is significantly faster compared to the common solid state furnace diffusion. Immediately within 100 ns after the laser pulse, silicon quickly recrystallizes epitaxially, while the dopant atoms are incorporated into the crystal. The ratio of dopant concentrations directly at the liquid/solid interface defines the (equilibrium) partitioning coefficient $k_{\text{eq}} = C_s/C_l$, with the concentrations in the Si crystal, C_s , and melt, C_l , for infinitely slow solidification. For high solidification velocities, *solute trapping* occurs and the effective partition coefficient k_{eff} deviates from the equilibrium value towards unity.

We investigate the boron (B) and antimony (Sb) incorporation and redistribution during repeated laser melting. Our numerical model yields simulated profiles which excellently agree with the secondary ion mass spectroscopy (SIMS) measurements. Consequently, we determine the effective B and Sb partitioning coefficients, which are significantly larger than their respective equilibrium values $k_{\text{eq}}^{\text{B}} = 0.8$ and $k_{\text{eq}}^{\text{Sb}} = 0.023$.²⁸

²⁸R. F. Wood, "Model for nonequilibrium segregation during pulsed laser annealing," Applied Physics Letters **37**, 302–304 (1980).

Figure 2.20a) shows boron profiles, which exhibit a distinct pile-up at the maximum melt-depth, due to *solute trapping* effects indicated by $k_{\text{eff}}^{\text{B}} = 1.25$. Figure 2.20b) depicts the respective antimony profiles, which almost coincide due to the surface segregation of antimony. Nevertheless, the effective partitioning coefficient $k_{\text{eff}}^{\text{Sb}} = 0.75$ indicates a strong influence of *solute trapping*. For all three pulse energies $E_{\text{p}1} = 190 \mu\text{J}$, $E_{\text{p}2} = 230 \mu\text{J}$, $E_{\text{p}3} = 250 \mu\text{J}$ and constant number of laser scans $N_s = 40$, experimental and simulated profiles match excellently.

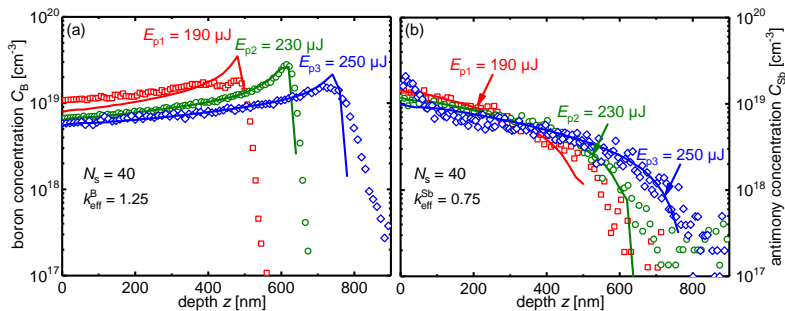


Figure 2.20: a) Experimental (open symbols) and simulated (lines) boron (B) concentration profiles exhibit pile-up at maximum melt depth and b) antimony (Sb) concentration profiles show surface segregation. The simulation reproduces the experimental data very well for all three laser pulse energies E_{p} at constant number of laser scans N_s . The determined effective partitioning coefficients $k_{\text{eff}}^{\text{B}}$ and $k_{\text{eff}}^{\text{Sb}}$ reveal the influence of solute trapping for laser melting and resulting rapid solidification.

Our approach offers a simple and straightforward procedure to determine the partitioning coefficient from experimental results. Additionally, for any known dopant data the final concentration profiles can be obtained with our model and be used for profile optimization trials, thereby minimize the experimental effort.

Design of a Dielectric Barrier Discharge Plasma Reactor for CO₂-Reduction

Stephan Renninger

**In collaboration with: Friedrich Speckmann and
Kai Peter Birke**

The conversion of carbon dioxide (CO₂) and hydrogen (H₂) to hydrocarbons opens new ways of storing renewable energies. Plasma technology has been demonstrated as a viable way of carbon dioxide reduction to monoxide (CO), which is an important step in this process.

Dielectric barrier discharge (DBD) plasmas are scalable and operate at atmospheric pressure, making them attractive for industrial use. However, observed efficiencies remain insufficient. To study them further, a test rig is designed which allows the measurement of electrical, thermal, and internal energy of processed gasses. Gathered data will be used in parameter studies and simulation.

The breakdown field strength of CO₂ of $E_b = 6 \text{ kV/mm}$ necessitates a DC source voltage $U_{\text{nom}} = E_b d_g$ where the electrode gap is d_g . Square wave voltages are produced using a half bridge consisting of two MOSFETs, resistors limit the switching currents. The maximum frequency is limited by available current, since charge stored in the electric field of the dielectric C_d is dissipated after each pulse.

The maximum required current is $I_{\text{req}} = f_{\text{DBD}} Q_p = f_{\text{DBD}} \Delta U C_d$, $\Delta U < U_{\text{nom}}$ is the discharge voltage window and Q_p the charge used each period.²⁹ Typical operation range of DBD plasmas is $f_{\text{DBD}} = 0,5...100\text{ kHz}$. Measurement of thermal and internal energy is achieved with gas flow, pressure, and temperature sensors. Exhaust gas is characterized using gas spectroscopy. The ratio of electrical power consumed and gas flow is adjusted to gas conversion rate, energetic efficiency, and temperature limits of the facility. In further development a selective oxygen ion conducting membrane will be employed. The removal of oxygen is thought to shift chemical equilibrium, thus increasing conversion rate.

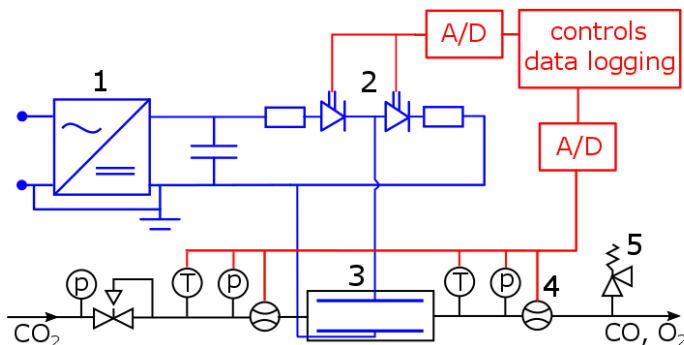


Figure 2.21: Proposed test facility for DBD-Plasma characterization; shown are plumbing (black), signal & measurement (red) and power electronics (blue). 1: HV-DC Source. 2: half bridge. 3: plasma chamber. 4: flow rate sensor. 5: bleeder valve.

²⁹S. Liu & M. Neiger, "Electrical modelling of homogeneous dielectric barrier discharges under an arbitrary excitation voltage", Journal of Physics D: Applied Physics **36**, 3144 (2003).

Quantitative Validation of Calendar Aging Models for Lithium-Ion Batteries

Severin Hahn

Service life will be a key parameter to achieve deep market penetration for EVs. While exhaustive it is possible to test the entire energy throughput of a battery or cell and thus its cyclic aging. Testing for calendaric aging over lifetime, however, is infeasible. Thus, accurate and robust calendar aging models predicting lifetime are highly important due to quality assurance, warranty and even regulatory requirements.

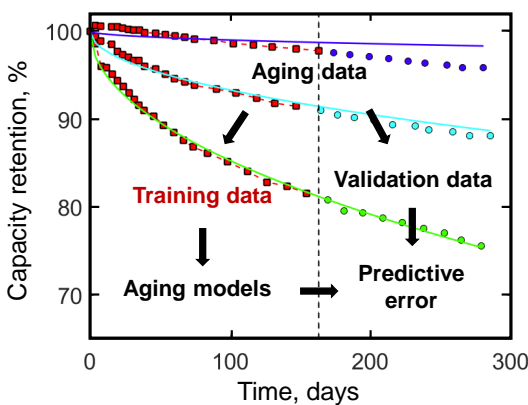


Figure 2.22: Validation method overview for calendar aging models. Aging data is split in training and validation data, where models are fitted to training data but evaluated against validation data to measure predictive capability. Reproduced from Hahn et al.³⁰ with permission of Elsevier.

Many calendar aging models have been developed, most of which are based on the famous $t^{0.5}$ relationship and fitted to data with free parameters. However, quantitatively comparative studies of aging models often have been limited to the model's goodness of fit R^2 , critically favoring adaptive, overfitting models. We introduce a new technique to quantify the predictive ability of calendar aging models³⁰ where the aging data set is split into training and subsequent validation data as shown in Fig. 2.22. The aging model is fitted to training data, but evaluated against both training and validation data. The error to validation data is thus able to quantify the models predictive capability. In fact, the validation technique may detect overfitting models, which fit great to training data but are less successful predicting validation data.

Additionally, we propose a new aging model based on theoretical considerations on the effect of the initial SEI during formation. The introduced parameter of lithium lost to the initial SEI is measured experimentally by two distinct matching methods.

The comparative study is based on a calendar aging matrix consisting 54 automotive pouch cells which were used in the EV 'smart electric drive' by Daimler. The validation technique is used to quantitatively compare the proposed model to five competing models from literature. Indeed, the proposed model surpasses literature models in terms of predictive capability. In conclusion, both the proposed aging model and the validation technique are useful tools to be used in further development of calendar aging models.

³⁰S. L. Hahn et al., "Quantitative validation of calendar aging models for lithium-ion batteries", Journal of Power Sources **400**, 402–414 (2018).

Thermal Propagation in Lithium-Ion Traction Batteries

Sascha Koch

In collaboration with: Alexander Fill, Kai Peter Birke

With battery electrical vehicles becoming more and more prominent in the transportation market, concerns about safety rise. Overheating, caused by manufacturing errors, misuse or wrongly chosen operating conditions leads lithium-ion cells into undesired internal chemical reactions, which lead to massive amounts of excess heat and flammable venting gas. Without appropriate counter measures these reactions trigger neighboring cells and cause a chain reaction. The omnipresent tendency to higher energy densities and capacities further increase this danger. Figure 2.23 illustrates this chain reaction. Starting on the left side with a single cell going into so called thermal runaway (TR) exothermic chemical reactions and the internal discharge of the electrically stored energy create huge amounts of excess heat that can get transferred to adjacent cells. If these neighboring cells hereby exceed a certain trigger temperature, they themselves go into TR . Displayed on the very right, this spreading of TR is called Thermal Propagation. If not handled properly, results might include melting battery housings, ignition of venting gas, electric arcs and possible explosion of the battery. Gas analysis delivers useful insights into gas composition and the influence of varying cell parameters on the venting gas.³¹ Most im-

³¹S. Koch et al., "Comprehensive gas analysis on large scale automotive lithium-ion

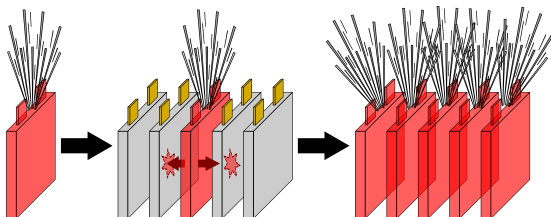


Figure 2.23: Process of thermal propagation. Starting with a single cell thermal runaway, producing venting gas and excess heat, neighboring cells are overheated and therefore also triggered to undergoing a thermal runaway.

portantly, energy density and cell capacity are found to have an aggravating effect on total amount of released venting gas as well as cell mass loss during TR. Further, the share of gas mass and solid particles on total mass loss depends on cell housing, pouch cells tend to lose a greater portion of mass in gaseous form than hard case cells. Unaffected by the amount of released gas during TR, the gas composition is relatively stable with carbon dioxide, carbon monoxide and hydrogen as the three most common components. In order to build competitive batteries with high energy density cells and still guarantee passenger safety, a warning system is developed. This system provides passengers information about a potential safety threat from a starting TP in the lithium-ion battery in their vehicle, we evaluate the feasibility of different sensors for a TR detection system.³² A combination of two or more sensors are found to be necessary, to form a detection system with a high detection speed and a clear signal.

cells in thermal runaway”, Journal of Power Sources **398**, 106–112 (2018).

³²S. Koch et al., “Fast thermal runaway detection for lithium-ion cells in large scale traction batteries”, Batteries **4** (2018) 10.3390/batteries4020016.

Differential Fourier Imaging for Bioanalytics

Markus Schubert

In collaboration with: Marcel Berner, Sascha Koch,
Johannes Siegel, and Biometrics GmbH

Many data projectors nowadays use powerful Digital Mirror Devices (DMDs). Such DMDs give us the chance to transform optical signals from various measurement spots in microfluidic channels of a bioanalytical device into corresponding channels in the frequency domain, and thereby enable highly sensitive detection of small differences between analyte and reference signals. Our novel Differential Fourier-transform Imager (DFI) replaces expensive cameras in Reflectometric Interference Spectroscopy (RIfS) by a DMD and a simple photodetector.³³ Figure 2.24 illustrates the working principle of the DFI, sketching our experimental setup.³⁴ The DMD control selects spots of interest on the microfluidic device, i.e. locations $x_1 \dots x_n$ with defined shapes and areas. The RIfS signals from those spots are amplitude modulated (AM) by the DMD at corresponding carrier frequencies $f_1 \dots f_n$. Our experimental setup implements AM modulation by a pulse-width modulation of the DMD mirror movement. Only a single photodetector is needed for recording all superimposed optical signals at once.

³³M. Berner, G. Gauglitz, U. Hilbig, S. Koch and M. Schubert, *Method and device for the spatially resolved measurement of radiation signals*, Patent, DE102016113703, WO002018019666, 2016.

³⁴S. Koch, *Machbarkeitsnachweis des Fourier Transform Imager*, Masterarbeit, Universität Stuttgart, *ipv*, 2016.

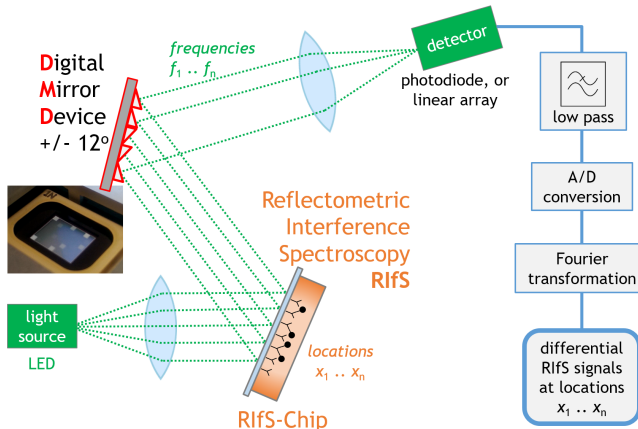


Figure 2.24: Laboratory setup for evaluating Differential Fourier Imaging for the bio-analytical method RIfS. The Digital Mirror Device DMD transforms the reflected light originating from locations $x_1 \dots x_n$ on the microfluidic RIfS chip into corresponding AM signals at carrier frequencies $f_1 \dots f_n$. The photodetector provides input for the signal processing chain, which finally delivers differential RIfS signals between arbitrarily defined areas of interest in the microfluidic channels.

Bandwidth limitation of the photodetector output and high-resolution analog-digital conversion provide input data for the final Fourier transformation that separates the RIfS signals originating from $x_1 \dots x_n$. High sensitivity differential measurements between any of two locations x_k and x_k simply result from phase-shifting the DMD modulation, i.e. choosing $f_k = f_m$ with a 180 degree phase shift. For evaluating the potential and performance of the DFI, we first use an LCD screen to simulate the optical signal input from the microfluidic channels. Signal differences as low as a grey scale change by 150 out of 256 bits of one single LCD pixel inside a detection area of 100 by 100 pixels are reliably discriminated.

Fourier Imaging of Microfluidic Channels

Johannes Siegel

In collaboration with: Chenyang Zhang, Markus Schubert, and Biometrics GmbH

Starting from a first laboratory setup for Differential Fourier Imaging (DFI) that is described elsewhere in this annual report, careful optimization of the optical path boosts its throughput by a factor of 300. This improvement facilitates to proceed to first differential Reflectometric Interference Spectroscopy (RIfS)³⁵ measurements between separate microfluidic channels, and to start evaluating the performance of our novel DFI method for RIfS applications. RIfS is a versatile, direct-optic bioanalytical tool that covers a wide range of applications.³⁶ Enhancing RIfS by DFI, not only opens pathways to low-cost, high-volume screening of virus infections, food or water contaminants, but also to high-quality analytics of sophisticated multi-analyte assays. The substantial improvement of the optical setup relies on a complete ray-tracing model, on consecutive removal of all impeding limitations, and on continuous monitoring of the results by applying statistical measures to the output of the fully computer-controlled measurement sequences.³⁷ Figure 2.25

³⁵G. Gauglitz et al., "Chemical and biochemical sensors based on interferometry at thin (multi-) layers", Sensors and Actuators B: Chemical **11**, 21–27 (1993).

³⁶Biometrics GmbH, Tübingen, Website, <http://biometrics.com/applications/>.

³⁷R. Rösch, *Entwicklung einer automatisierten Testumgebung für ein optisch moduliertes Imaging-System, Masterarbeit, Universität Stuttgart, ipv, Masterarbeit, Universität Stuttgart, ipv*, 2017.

presents a test for evaluating sensitivity, linearity and noise versus measurement speed by analyzing consecutive step-ups in NaCl concentration c_2 in the microfluidic channel Ch2 while the reference concentration c_1 in channel Ch1 remains at $c_1 = 0\%$. Since RIfS relies upon refractive index changes by selective attachment of biomolecules to the functionalized inner surface of the RIfS channel, simple testing by stepwise raising of the refractive index of the flowing agent is an adequate method for qualifying our DFI-RIfS setup. Future developments strive for DFI-RIfS investigations of *real* bioanalytical assays of our industrial partner Biometrics GmbH. The existing laboratory setup will become portable soon, and later implementation of lock-in detection and analysis of local spectral information open a vast field of innovative DFI-RIfS designs.

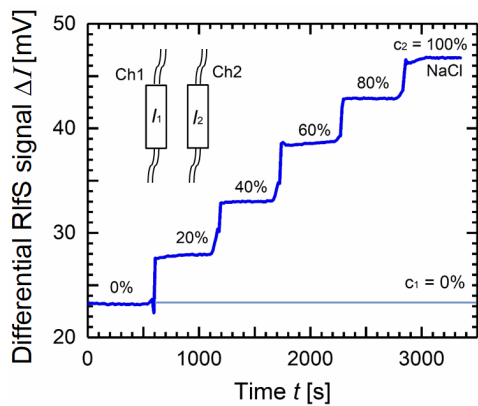


Figure 2.25: Result of testing DFI-RIfS from microfluidic channels: Pure water and saline solution NaCl are pumped through two microfluidic channels Ch1 and Ch2 with the same flow rate $s_1 = s_2 = 30 \mu\text{l}/\text{min}$. Our DFI-RIfS setup acquires both intensities I_1 and I_2 , and calculates the differential RIfS signal $\delta I = I_2 - I_1$ while the NaCl concentration in Ch2 steps up from $c_2 = 0\%$ to $c_2 = 100\%$.

3 Publikationen | Publications

- F. Dreyer, N. Hoppe, J. Köhler, W. Vogel, M. Dahlinger, M. Félix Rosa, L. Rathgeber, J. Werner and M. Berroth, "Schottky-Fotodioden basierend auf laserkristallisierten Germanium-Schichten", in URSI-KH2017-Programm (Union Radio Scientifique Internationale (U.R.S.I.): Kleinheubacher Tagung 2017, Sep. 2017), S. 45, 46.
- C. Sämann, K. Kelesiadou, S. S. Hosseinioun, M. Wachtler, J. R. Köhler, K. P. Birke, M. B. Schubert and J. H. Werner, "Laser porosified silicon anodes for lithium ion batteries", Advanced Energy Materials **8**, 1701705 (2018).
- F.-W. Speckmann, D. Müller, J. Köhler and K. P. Birke, "Low pressure glow-discharge methanation with an ancillary oxygen ion conductor", Journal of CO₂ Utilization **19**, 130–136 (2017).
- P. C. Lill, M. Dahlinger and J. R. Köhler, "Boron partitioning coefficient above unity in laser crystallized silicon", Materials **10**, 189 (2017).
- K. Carstens, M. Dahlinger, E. Hoffmann, R. Zapf-Gottwick and J. H. Werner, "Amorphous silicon passivation for 23.3% laser processed back contact solar cells", Japanese Journal of Applied Physics **56**, 08MB20 (2017).
- J. Nover, R. Zapf-Gottwick, C. Feifel, M. Koch, J. W. Metzger and J. H. Werner, "Reply to "comment on long-term leaching of photovoltaic modules"" , Japanese Journal of Applied Physics **57**, 019102 (2018).
- J. Nover, R. Zapf-Gottwick, C. Feifel, M. Koch, J. W. Metzger and J. H. Werner, "Long-term leaching of photovoltaic modules", Japanese Journal of Applied Physics **56**, 08MD02 (2017).

T. Kropp, M. Schubert and J. H. Werner, "Quantitative prediction of power loss for damaged photovoltaic modules using electroluminescence", *Energies* **11**, 1172 (2018).

M. Berner, U. Hilbig, M. B. Schubert and G. Gauglitz, "Laser-induced fluorescence detection platform for point-of-care testing", *Measurement Science and Technology* **28**, 085701 (2017).

F. Baldini, C. Berrettoni, A. Giannetti, S. Tombelli, C. Trono, G. Porro, R. Bernini, I. A. Grimaldi, G. Testa, G. Persichetti et al., "Novel fluorescence-based pocf platform for therapeutic drug monitoring in transplanted patients (conference presentation)", in *Optical diagnostics and sensing xvii: toward point-of-care diagnostics*, Bd. 10072 (International Society for Optics and Photonics, 2017), S. 100720C.

T. Menold, M. Ametowobla, J. Köhler and J.H. Werner, "Surface patterning of monocrystalline silicon induced by spot laser melting", *Journal of Applied Physics* **124**, 163104 (2018).

T. Kropp, M. Berner and J. H. Werner, "Self-scaling minority carrier lifetime imaging using periodically modulated electroluminescence", *Journal of Applied Physics* **122**, 183105 (2017).

M. Dahlinger, *Laserprozessierte Rückkontakt-Solarzellen aus Silizium*, 978-3-8439-3746-7 (Verlag Dr. Hut, München, Deutschland, 2017).

K. Carstens, *Passivierung kristalliner Silizium-Solarzellen mit amorphem Silizium*, 978-3-8439-3328-5 (Verlag Dr. Hut, München, Deutschland, 2017).

C. Sämann, *Laserporosierte Siliziumanoden für Lithium-Batterien*, 978-3-8439-3746-7 (Verlag Dr. Hut, München, Deutschland, 2018).

- A. U. Schmid, L. Lindel and K. P. Birke, "Capacitive effects in $\text{Li}_{1-x}\text{Ni}_{0.3}\text{Co}_{0.3}\text{Mn}_{0.3}\text{O}_2-\text{Li}_x\text{C}_y$ Li-ion cells", *Journal of Energy Storage* **18**, 72–83 (2018).
- A. U. Schmid, L. Eringer, I. Lambidis and K. P. Birke, "Electrochemical balancing of lithium-ion cells by nickel-based cells", *Journal of Power Sources* **367**, 49–56 (2017).
- S. Koch, A. Fill and K. P. Birke, "Comprehensive gas analysis on large scale automotive lithium-ion cells in thermal runaway", *Journal of Power Sources* **398**, 106–112 (2018).
- A. Fill, S. Koch, A. Pott and K. P. Birke, "Current distribution of parallel-connected cells in dependence of cell resistance, capacity and number of parallel cells", *Journal of Power Sources* **407**, 147–152 (2018).
- J. P. Singer, T. Kropp, M. Kuehnemund and K. P. Birke, "Pressure characteristics and chemical potentials of constrained $\text{LiFePO}_4/\text{C}_6$ cells", *Journal of The Electrochemical Society* **165**, A1348–A1356 (2018).
- J. Singer, C. Sämann, T. Gössl and K. P. Birke, "Pressure monitoring cell for constrained battery electrodes", *Sensors* **18**, 3808 (2018).
- S. L. Hahn, M. Storch, R. Swaminathan, B. Obry, J. Bandlow and K. P. Birke, "Quantitative validation of calendar aging models for lithium-ion batteries", *Journal of Power Sources* **400**, 402–414 (2018).
- N. Bouchhima, M. Schnierle, S. Schulte and K. P. Birke, "Optimal energy management strategy for self-reconfigurable batteries", *Energy* **122**, 560–569 (2017).

- J. P. Singer and K. P. Birke, "Kinetic study of low temperature capacity fading in li-ion cells", *Journal of Energy Storage* **13**, 129–136 (2017).
- S. Koch, K. P. Birke and R. Kuhn, "Fast thermal runaway detection for lithium-ion cells in large scale traction batteries", *Batteries* **4**, 16 (2018).
- C. Bolsinger, M. Zorn and K. P. Birke, "Electrical contact resistance measurements of clamped battery cell connectors for cylindrical 18650 battery cells", *Journal of Energy Storage* **12**, 29–36 (2017).
- F.-W. Speckmann, S. Bintz, M. L. Groninger and K. P. Birke, "Alkaline electrolysis with overpotential-reducing current profiles", *Journal of The Electrochemical Society* **165**, F456–F462 (2018).
- N. Bouchhima, M. Gossen, S. Schulte and K. P. Birke, "Lifetime of self-reconfigurable batteries compared with conventional batteries", *Journal of Energy Storage* **15**, 400–407 (2018).
- C. Bolsinger, J. Brix, M. Dragan and K. P. Birke, "Investigating and modeling the transmission channel of a prismatic lithium-ion cell and module for powerline communication", *Journal of Energy Storage* **10**, 11–19 (2017).
- K. P. Birke, "Zukunft Lithium-Ionen-Akku Bewertungsmaßstäbe auf dem Prüfstand", *ATZelektronik* **13**, 16–23 (2018).
- K. P. Birke, "The future of the lithium-ion battery assessment standards on the test bench", *ATZelektronik worldwide* **13**, 16–21 (2018).
- C. Bolsinger and K. P. Birke, "Effect of different cooling configurations on thermal gradients inside cylindrical battery cells", *Journal of Energy Storage* **21**, 222–230 (2019).

3 Publikationen | Publications

P. Kölblin, M. Schubert, J. H. Werner and M. Reuter, "Data acquisition of defects in pv power plants based on electroluminescence images", in *Proc. of the 6th International Education Forum on Environment and Energy Science* (Dez. 2017).

J. Nover, R. Zapf-Gottwick, C. Feifel, M. Koch, J. W. Metzger and J. H. Werner, "Identifying weak spots in photovoltaic modules during long-term leaching", in *Proc. of the 6th International Education Forum on Environment and Energy Science* (Dez. 2017).

T. Kropf, M. Berner and M. Schubert, "High resolution carrier lifetime imaging", in *Proc. of the 6th International Education Forum on Environment and Energy Science* (Dez. 2017).

4 Was sonst noch war... | Beyond Science...



Brigitte Lutz und Leonhard Bauer gehen in Rente

Nach über 40 Jahren am *ipv* genießt Brigitte seit Ende September 2017 ihren wohlverdienten Ruhestand.

Leo verließ uns Ende Juli 2018; er kommt jetzt nur noch zu Besuch und gibt Tipps, wenn eine in die Jahre gekommene Anlage streikt.

ETI Cup 2018

Nach 9 Jahren hat das *ipv*-Fußballteam den ETI-Pokal wieder nach Hause geholt. Mit einem 1:0 gegen die Auswahlmannschaft dreier Institute haben unsere Jungs im Endspiel gezeigt, was sie können.

Reinraumumbau

Ursprünglich sollte unser Reinraumumbau spätestens bis Mitte April 2017 abgeschlossen sein. Dass dies immer noch nicht der Fall ist, liegt vermutlich an nicht definierten Zuständigkeiten der am Umbau beteiligten Organisationen und Personen.

Brigitte Lutz and Leonhard Bauer retire

After more than 40 years at the institute, Brigitte has been enjoying her well-deserved retirement since the end of September 2017.

Leo left us at the end of July 2018. He now only comes to visit us and gives us tips when an old apparatus goes on strike.

ETI Cup 2018

After 9 years, the *ipv* football team has brought the ETI Cup home again. With a 1:0 against the selection team of three institutes, our boys showed in the final what they are capable of.

Retrofit of the Cleanroom

Originally, our cleanroom retrofit was to be completed by mid-April 2017 at the latest. This is still not the case, probably due to undefined responsibilities of the organizations and persons involved in the retrofitting.

Sommerfeste 2017 und 2018

Wie jedes Jahr gab es auch 2017 und 2018 zum Ende des Sommersemesters ein Grillfest, zu dem nicht nur die Mitarbeiter des *ipv*, sondern auch Ehemalige und natürlich auch „unsere“ Studenten eingeladen waren. Auf Grund des extrem trockenen 2018er Sommers durften wir in diesem Jahr wegen „Waldbrandgefahr“ leider nicht auf unserer *ipv*-Wiese grillen, sondern mussten mit dem Innenhof der ETI-Gebäude Vorlieb nehmen.

ACCEEES Forum 2017

Beim *6th International Education Forum on Environment and Energy Science* erhielt Timo Kropp den Preis für den besten wissenschaftlichen Vortrag. Dieses Forum wird von der *Academy for Co-creative Education of Environment and Energy Science (ACEEES)* des *Tokyo Institute of Technology* veranstaltet.

Summer Barbecues 2017 and 2018

As every year, there was a barbecue in 2017 and 2018 at the end of the summer semester to which not only the *ipv* staff, but also alumni and, of course, „our students“ were invited. Due to the extremely dry summer 2018, we were unfortunately not allowed to barbecue on our *ipv* lawn this year due to the danger of „forest fires“. Thus, we used the inner courtyard of the ETI buildings.

ACCEEES Forum 2017

At the *6th International Education Forum on Environment and Energy Science* Timo Kropp received the award for the best scientific lecture. This forum is organized by the *Academy for Co-Creative Education of Environment and Energy Science (ACEEES)* of the *Tokyo Institute of Technology*.

Stuttgarter Photovoltaikpreise 2017

Wie in den Jahren zuvor verlieh der Förderverein der Freunde des Instituts für Photovoltaik VF-*ipv* am 25.01.2018 die *Stuttgarter Photovoltaik Preise 2017* im Rahmen eines Fest-Kolloquiums. Prämiert wurden drei herausragende studentische Arbeiten.

Die Preisträger des Jahres 2017 sind:

The laureates of the year 2017 were:

Bachelorarbeiten/Bachelor Thesis:

Nathanael Becker

Forschungsarbeiten/Research Thesis:

Kevin J. Roberts

Masterarbeiten/Master Thesis:

Pascal Kölblin



Stuttgart Photovoltaics Award 2017

As in previous years, on 25 January 2018, the association VF-*ipv* "Freunde des Instituts für Photovoltaik" (Friends of the Institute for Photovoltaics) bestowed the *Stuttgart Photovoltaics 2017 Award* in a festive colloquium. Three outstanding student works were awarded.

5 Lehrveranstaltungen | Lectures

Mikroelektronik I (Bachelor, Wintersemester)

J. H. Werner

- Energiebänder und Leitfähigkeit
- Silizium – der Werkstoff der Mikroelektronik
- Elektronen und Löcher in Halbleitern
- Ströme in Halbleitern
- Nichtgleichgewicht, Injektion, Extraktion
- Elektrostatik des pn-Übergangs
- Ströme im pn-Übergang

Einführung in die Elektrotechnik für Kybernetik und Verkehrsingenieurwesen (Bachelor, Sommersemester)

K. P. Birke

- Elektrischer Gleichstrom
- Wechselstrom
- Elektrische und magnetische Felder

Photovoltaik I (Bachelor, Sommersemester)

J. H. Werner

- Der Photovoltaische Effekt:
Solarzelle, -modul, -anlage
- Sonnenspektrum und -leistung,
Energieverbrauch in Deutschland
- Maximaler Wirkungsgrad von Solarzellen
- Ersatzschaltbilder
- Photovoltaik-Materialien und -Technologien
- Modultechnik

- Photovoltaic System Technology

Optoelectronics I (Bachelor, Sommersemester)

J. H. Werner

- Generation and transport of radiation
- Coherence
- Semiconductor basics
- Excitation and recombination processes
- Light emitting diodes
- Semiconductor lasers
- Glass fibers
- Photodetectors

Lasers and Light Sources (Master, Wintersemester)

J. H. Werner and J. R. Köhler

- Basics of light and generation of radiation
- Human vision
- Color
- Photometry
- Incoherent light sources
- Light emitting diodes
- Laser and laser processing

Photovoltaik II (Master, Wintersemester)

J. H. Werner

- Solar radiation
- Alternatives to conventional silicon cells
- Market and economic viability of photovoltaic power plants
- Planning, installation, operation and monitoring of photovoltaic power plants
- Location and shading

5 Lehrveranstaltungen | Lectures

- Komponenten von Photovoltaikanlagen
- Simulationen
- Photovoltaische Messtechnik

Battery Modelling and Energy Management (Master, Wintersemester)

K. P. Birke

- Electrical battery models
- Aging effects in batteries
- Thermal battery models
- Implementation of battery models
- Energy management
- Sustainable energy chains
- Smart house
- Future concepts for battery modelling and energy management

Photovoltaik III (Master, Sommersemester)

J. H. Werner

- Solarstrahlung und Absorption
- Elektronischer Transport in Halbleitern
- Rekombinationsprozesse in Halbleitern
- Theorie der idealen Solarzelle
- Wirkungsgradgrenzen von Silizium
- Optische Eigenschaften von Solarzellen
- Oberflächen, Grenzflächen und Kontakte

Werkstoffe der Elektrotechnik (Master, Wintersemester)

K. P. Birke

- Aufbau und Eigenschaften der Materie

5 Lehrveranstaltungen | Lectures

- Kristallstruktur in Festkörpern, Eigenschaften von Flüssigkeiten und Gasen
- Werkstoffzusammensetzung und Mikrogefüge
- Metallische Werkstoffe
- Dielektrika
- Keramische Werkstoffe
- Magnetismus, dia-, para-, ferro- und antiferromagnetische Werkstoffe und zugrunde liegenden Effekte
- Ferro- und pyroelektrische Werkstoffe und ionenleitende und gemischt elektrisch/ionenleitende Feststoffe
- Organische Werkstoffe

Mobile Energiespeicher (Bachelor/Master, Wintersemester)

K. P. Birke

- Elektrifizierung des Antriebsstrangs, Architekturen
- Elektrische Energiespeicher für Elektromobilität
- Batteriemanagement und Ladekonzepte
- Systemarchitekturen
- Elektromobilität: Gesamtenergiebilanzbetrachtungen, Recycling, Umweltaspekte, Kostenstrukturen, Akzeptanz
- Weitere Applikationen: Schiene, Luftfahrt, Schiffe

Photovoltaische Inselsysteme (Bachelor/Master, Wintersemester)

B. Zinßer

- Funktionsweise von photovoltaischen Inselsystemen
- Typen von Inselsystemen und deren Komponenten
- Simulationsverfahren
- Wirtschaftlichkeit
- Auslegung

Speichertechnik für elektrische Energie I
(Bachelor/Master, Sommersemester)

K. P. Birke

- Aufbau und Funktionsweise von elektrischen, elektromechanischen und elektrochemischen Speichern
- Charakterisierung der Speicher

Wissenschaftliches Vortragen und Schreiben I
(Bachelor/Master, Wintersemester)

J. H. Werner

- Kernbotschaften
- Aufbau eines Vortrags
- Standardfehler (Strukturfehler, Technikfehler, Fehler im Auftreten)
- Praktische Schritte zum Vortrag
- Präsentation eines wissenschaftlichen Vortrages von 12 min. (mit Videoaufzeichnung)
- Selbst- und Fremdbeurteilung

Wissenschaftliches Vortragen und Schreiben II
(Bachelor/Master, Wintersemester)

J. H. Werner

- Kernbotschaften
- Aufbau und Elemente einer Publikation
- Bilder, Tabellen, Gleichungen und Referenzen
- Verfassen eines eigenen wissenschaftlichen Kurzberichts von 4 bis 6 Seiten

Speichertechnik für elektrische Energie II (Bachelor/Master, Sommersemester)

K. P. Birke

- Elektrische Energiespeicherzellen
- Energiespeichersysteme
- Speicher-Management (Messen, Steuern, Regeln)
- Simulation
- Großtechnische elektrochemische und chemische Energiespeicherung

Engineering Materials (Bachelor/Master, Wintersemester)

K. P. Birke

- Atom and ion movements (diffusion) in materials
- Thermal properties of materials
- Ceramic materials
- Polymers
- Electronic materials
- Examination and characterization of materials
- Application

Fachpraktikum „Messtechnik für Energiewandler und Energiespeicher“ (Master, Wintersemester)

Fachpraktikum „Photonik und Energiewandler“ (Bachelor, Sommersemester)

Grundlagenpraktikum (Bachelor, Sommersemester)

Praktikum „Erneuerbare Energien“, Versuch 1: Photovoltaik (Bachelor, Sommersemester)

6 Abschlüsse | Degrees

Promotionen | PhD Theses



Dahlinger, Morris

Laserprozessierte Rückkontakt-Solarzellen aus Silizium

Carstens, Kai

Passivierung kristalliner Silizium-Solarzellen mit
amorphem Silizium

Sämann, Christian

Elektrodenmaterialien für Li-Ionen-Akkumulatoren

Stoicescu, Liviu-Mihai

Bildgebende Messung der Lumineszenz von
Photovoltaikanlagen unter Tageslicht

Bachelorarbeiten | Bachelor Theses

Becker, Nathanael

Skalierbare Kühlsysteme für Gambia

Berliner, Noemi

Untersuchung der Schichthaftung von nanokristallinen Diamantschichten auf vorbehandelten Silizium-Substraten

Bux, Jonas

Inbetriebnahme eines DBD-Plasmasytems zur CO₂-Reduktion und Methanisierung

Dai, Wenjing

Stabilität von Ethylen-Vinyl-Acetat

Demartin, Elias

Untersuchungen zu neuartigen, geschlossenen Aluminium- Primärzellen

Ebeling, Sven

Hardwaretechnische Erweiterung eines Batteriemanagementsystems

Eckardt, Sebastian

Energiemanagement für Fliegen mit Photovoltaik

Epple, Simon

Moderne Serverarchitektur zur Überwachung dezentraler Energieerzeugungsanlagen

Höhn, Julia

High-Efficiency Solar Modules for Optical Power Transmission

Horch, Joachim

Photovoltaikanlagen mit optischen Reflektoren

Hund, Philipp

Optimierung von Siliziumnitrid-Passivierschichten

Jaworski, Peter

Ansteuerung eines Lasersystems für die Herstellung von
Hocheffizienz-Solarzellen

Kasrawi, Rabee

Messung elektrischer Kenngrößen von Photovoltaikmodulen

Klötzl, Nico

Strom/Spannungs-Charakterisierung defekter Solarmodule

Kovacheska, Mihaela

Laser-IBC Solarzellen mit texturierter Rückseite

Lachab, Ahmed

Mechanische Stabilität von Laser-verschweißten Aluminium-Kontakten
als Busbars auf Laser-IBC Solarzellen

Mavridis, Petros

Aktivierung von Antimon in Germanium durch Laser-Annealing

Mögle, Tobias

Charakterisierung eines Messchucks für
Rückseitenkontakte solarzellen

Ott, Viktor

Kameraansteuerung für die ortsaufgelöste Aufnahme von Elektro-
lumineszenzbildern von Solarmodulen

Reiser, Benedikt

Programm zum Entwurf beliebig geformter Solarmodule

6 Abschlüsse | Degrees

Schmid, Matthias

Pulsstromquelle für die Charakterisierung von Solarzellen

Schröter, Philipp

Untersuchung und Implementierung eines zuverlässigen drahtlosen Sensornetzwerkes

Silvestri, Gianluca

Erneuerbare Energien in Zahlen und Zeitreihen

Wagner, Markus

Test und Optimierung eines selbsttragenden Batteriemoduls

Wang, Yun

Einfahren einer Siebdrucklinie zur Metallisierung von Solarzellen

Forschungsarbeiten | Research Theses

Al Assadi, Anwar

Entwurf einer nachhaltigen Energiespeicherung basierend auf Wasserstoff für eine stationäre und mobile Anwendung

Atas, Yasin

Auslegung und Aufbau eines Batteriemoduls

Ayar, Ömer

Untersuchung von Additiven für Festkörper-Kompositelektrolyte

Bai, Dongyue

Entwicklung einer Zustandsmaschine für die Schalteransteuerung eines 48 V-Bordnetzes

Barth, Tim

Entwicklung einer Messvorrichtung für wiederholbare Lumineszenz-messungen

Bil, Sebastian

Nutzung von chemisch separierten Kupfer-Legierungen als Stromkollektoren in Lithium-Metall-Zellen

Bless, Niklas

Konzepte zur Erweiterung eines BMS-Zellmodels für Anoden mit SiO-Anteil

Bodenschatz, Sebastian

Ausfallmechanismen von Li-Ionen Batterien für Power Tools – Eine vertiefende Untersuchung des Hauptausfallgrundes der analysierten Batteriepacks

Chen, Yunming

Influence of Wafer Thickness and Laser Pulse Repetition Rate for Laser Doping

Conradt, Rafael

Modellierung eines selbst-adaptierenden elektrischen Ersatzschaltbildes zur Zustandserkennung eines elektrochemischen Energiespeichers

Cosgun, Zübeyr

Analyse der Blasenentwicklung in einer Elektrolysezelle mittels Videoaufnahme

Dreyer, Frederik

Laserkristallisation von Germanium für Infrarot-Photodioden

Fan, Hongxuan

Untersuchung von Photovoltaikmodulen mit Defekten

Gaus, Jannis

Verfahren zur Strukturierung eines Gel-Kompositelektrolyten

Gerber, Dennis

Konzeptionierung und Bau eines Prototyps eines Patchwork-Modules unter Berücksichtigung von System Anforderungen und Kosten

Geppert, Martin

Untersuchung alternativer Verarbeitungsmethoden von Feststoffionenleitern

Gesterkamp, Andreas

Experimentelle Bestimmung des Lithium-Plating-Verhaltens von Lithium-Ionen-Zellen bei Konstantstromladung

Gottberg, Luis

Improving the Quality of Silicon for Interdigitated Back Contact Solar Cells

Gries, Bastian

Evaluierung und Optimierung eines modularen Zellüberwachungssystems

Groninger, Max

Laserinduzierte Ausheilung von gesputterten Lithium-Mangan-Oxid Kathoden

Hasselwander, Samuel

Synthese eines Polymer-Keramik-Elektrolyten

Henger, Maximilian

Entwicklung eines optimierten Lastprofils zur konzeptionellen Auslegung von Traktionsspeichern in der Formel E

Heydgen, Julian

Entwicklung eines Kühlsystems für einen modularen Batteriespeicher

Kelesiadou, Katerina

Thermal Propagation Verhalten von parallel verschalteten Lithium-Ionen-Zellen

Kidane, Natnael

Auslegung eines Hochleistungs-/Hochenergiespeichers für die Elektrotraktion

Klaiber, Kevin

Entwicklung einer flexiblen Testfallspezifikation und Testautomatisierung für einen 48V HIL Powerpack-Prüfstand

Klöckner, Maximilian

Softwareumgebung zur Quantifizierung der Elektrolumineszenz von Solarmodulen

Koohi, Roya

Investigation of Laser Welding of the Current Collectors in a Battery

Kopp, Mike

Weiterentwicklung eines -Batteriemoduls zur druckabhängigen Zustandsbestimmung

Kreher, Tina

Simulation des Propagationsverhaltens von Solid-State-Zellen in Batteriemodulen

Kühnemund, Martin

Druckuntersuchung an Lithium-Ionen Zellen

Lambarth, Maike

Elektrochemische Analyse von Druckauswirkungen auf Lithium-Ionen-Zellen

Lauer, Joscha

Auslegung eines Photovoltaik-Systems für das Projekt „Christopher“ in Tansania

Lukas, Sebastian

Optimierung von Graphit-Elektroden für Lithium-Ionen-Zellen

Melilli, Walter

Untersuchung alternativer Energiespeichertechnologien für ein Routenzugsystem in der Intralogistik

Mögerle, Stephan

Wireless Sensor Gateway

Reich, Robert

Potenzialanalyse der anwenderbezogenen Variation von Betriebsparametern zur Steigerung der Performance von Elektrowerkzeugen und Akkumulatoren

Renninger, Stephan

Festelektrolyte in Lithiummetall-Zellen

Rieger, Jonathan

Technische und wirtschaftliche Bewertung eines stationären Batteriespeichers für Schnellladinfrastruktur von Elektrofahrzeugen

Roberts, Kevin John

Evaluierung und Implementierung eines energiesparenden, kapazitiven Tasters für akkubetriebene, mobile Applikationen

Sasanpour, Shima

Lösbare Kontaktierung von Lithium-Ionen Zellen mithilfe des Kaltgasspritzens

Schmid, Philipp

Sensorinterface zur Anbindung an drahtlose Kommunikationseinheit

Schmidt, Gerold

Herstellung von Graphitelektroden mit reduziertem Binderanteil für Lithium-Ionen-Batterien

Schirm, Thomas

Entwicklung und Aufbau einer Master-Unit für einen stationären Energiespeicher

Schößler, Torsten

Evaluation of an Asymmetric Concentrating Solar Photovoltaic Thermal (C-PVT) Installation

Schuchert, Christopher

Entwicklung eines Verfahrens zur Temperaturbestimmung von 18650 LiFePO₄-Zellen mit Hilfe künstlicher neuronaler Netze

Seitz, Josefine

Determination of the Nominal Module Operating Temperature (NMOT)

Siegel, Samuel

Konzeptabsicherung von Power CAPs als dezentrale Pufferspeicher in automobilen Energie-Bordnetzen

Stoll, Benedikt

Charakterisierung der Alterung von Lithium-Ionen-Zellen

v. Römer, Jacob

Konzeption und Aufbau einer Laserbearbeitungsanlage

Wagner, Lisa

Simulation und Auslegung von Relais und Sicherung im Batterie-Abschaltpfad

Wanner, Johannes

Implementieren von Basis-Funktionalitäten (Modulüberwachung) eines Basis BMS zur autonomen Überwachung eines Batteriemoduls

Weiblen, Maximilian

Softwaretechnische Implementierung einer Balancingstrategie

Winkler, Hui

Energy Harvesting Unit zum Betrieb drahtloser Sensoren

Wörle, Hubert

Moderne Verfahren zur Wasserstoffspeicherung und in-situ Erzeugung im automotiven Bereich

Ziegler, Theodor

Konstruktion eines Rolle-zu-Rolle Eloxierverfahrens von Aluminiumfolie

Zimmer, Jannik

Optimierung und Weiterentwicklung einer Batterie-Management-System-Workbench

Zimmermann, Lea

Auswirkung der Umwelteinflüsse auf Lumineszenzmessungen

Masterarbeiten | Master Theses

Anbalagan, Mathumathi

A Testbench with In-Place Design Validation for Smart EV Batteries

Bielmeier, Thomas

Wirtschaftliche Verbindungstechnologien für Zellen unterschiedlicher Formfaktoren für eine prototypische Fertigung

Bil, Sebastian

Untersuchung des Einflusses von Festkörperelektrolyten in Kombination mit strukturierten Ableitelektroden in Lithium-Metall Zellen

Bremersmann, Florian

Methodik zur Analyse und Optimierung des HV-Systems von Elektrofahrzeugen für das DC-Schnellladen

Chen, Qiang

Segmentierung der Bildverarbeitung von Lumineszenzmessungen an Photovoltaikmodulen

Demolli, Shkendije

Untersuchung der Wasserstofferzeugung über eine Lithium-Silizium-Legierung

Finke, Jonas

Aufbau eines echtzeitfähigen Batterietestsystems aus Standardkomponenten

Fitz, Oliver

Untersuchungen zur Wiederaufladbarkeit von Zink-Ionen-Zellen auf Basis saurer Elektrolyte für stationäre Anwendungen

Geifes, Florian

Aufbau und Implementierung eines Batteriespeichermodells zur Untersuchung im stationären Umfeld

Gesterkamp, Andreas

Untersuchung der Schnellladefähigkeit einer Lithium-Ionen-Zelle für Elektrofahrzeuge in Abhängigkeit des Zellalterungszustandes mit Hilfe von Drei-Elektroden-Zellen

Gössl, Tobias

Konstruktion einer Testzelle für Druckmessungen an Lithium-Ionen-Zellen

Gries, Bastian

Entwicklung eines 48 V Batteriemanagementsystems

Groninger, Max

Einfluss modifizierter Stromprofile auf einen alkalischen Elektrolyseur

Gün, Bahadir

A Battery Pack Simulation Hardware Driven By A Battery Cell Model

Hassan, Mohamed

Laser-Textured Diffraction Gratings for Improved Absorption of Solar Cells

Heim, Fabian

Alternative Bindematerialien für Lithium-Ionen Zellen

Horn, Alexander

Untersuchung fester Ionenleiter im Einsatz für Lithium-Batterien

Huang, Peng

Untersuchung von Photovoltaikerträgen über zehn Jahre

Jiang, Yufei

Construction and Comissioning of an Evaluation Platform for the Active Balancing Circiut

Khanof, Sogol

Nanoengineering YBa₂Cu₃O₇- superconducting thin films

Kleinheinz, Felix

Konzeptstudienentwicklung eines aktiven Stadtreinigungssystems im Elektroauto zur Verbesserung der Luftqualität in Metropolen

Koch, Fabian

Wasserstoffherstellung aus Silizium mit Natronlauge für mobile Anwendungen

Köblin, Pascal

Messtechnik für Photovoltaik-Testfeld im Projekt PARK

Koohi, Roya

Untersuchungen zum Laserstrahlfügen von Separatoren für Batteriezellen

Kraft, Matthias

Stabilität von Aluminium für die Verschaltung von Solarzellen im Modul

Kreher, Tina

Untersuchung strukturierter Stromableiter für Lithium-Metall-Elektroden

Laribi, Raoul

Untersuchung und qualitative Bewertung von Verfahren zur Lastkappung mittels Lithium-Ion-Batteriespeichern

Leins, Axel

Netzintegration E-Mobilität – Entwicklung eines Demonstrators für ein Smart-Home System

Lemke, Philip

Auslegung eines 48 V-Bordnetzspeichers mit 18650 Zellen

Li, Yuan

Entwicklung einer Lithium-Ionen-Batterie für den Antrieb eines Bootes

Limbach, Marius

Untersuchung der Auswirkungen von Pulsverfahren beim Laden und Entladen von Lithium-Ionen Zellen

Lindel, Lukas

Kapazitive Effekte in Lithium-Ionen-Zellen

Müller, Jonas

Synthese und Analyse eines Festkörper-Kompositeelektrolyten

Nüßle, Marius

Untersuchung der elektrochemischen Langzeitrelaxation von Lithium-Ionen-Zellen unter Verwendung eines elektrischen Zellmodells

Pang, Siyuan

Aufbau und Analyse eines CSC Systems mit dem LTC6813 Demo-board und Probefebetrieb mit einer Li-Ionen-Batterie

Renniger, Stephan

Verfahren zur makroskopischen Strukturierung eines Festkörper-Kompositelektrolyten

Rösch, Richard

Entwicklung einer automatisierten Testumgebung für ein optisch moduliertes Imaging-System

Schirm, Thomas

Entwicklung und Aufbau eines Batteriemoduls für einen stationären Batteriespeicher

Schuchert, Christopher

Impedanz-basierende Zustandsbestimmung von Lithium-Ionen-Zellen mit Hilfe künstlicher neuronaler Netze

Schwamm, Micha

Konzeption und Inbetriebnahme eines Gasmanagementsystems für mobile Applikationen

Stoll, Benedikt

Degradationsuntersuchung an metallisierten Folienkondensatoren

Tews, Alexander

Leistungsmultiplexer für Strom/ Spannungs-Kennlinienmessung

Tröger, Patrick

Aufbau eines Kennlinienmessplatzes für Photovoltaik-Modulstücke in Lösungen

Uhland, Thomas

Urbanisierung der Energiewende – Photovoltaik für Stuttgarter Schulen

Wang, Zuona

Entwicklung eines numerischen Modells zur thermischen Simulation von Batteriemodulen

Wanner, Johannes

Schätzung der inneren Zelltemperatur für Lithium-Eisenphosphat mithilfe neuronaler Netze

Xu, Yuheng

Aluminum-Metallization for Laser Back Contact Solar Cells

Zhang, Lu

Spatially resolved luminescence analysis of back contact solar cells

Zhang, Ruyin

Entwicklung einer In-Situ XRD-Messzelle für Zink-Luft-Batterien

Zhang, Tao

Entwicklung eines Mini-BMS auf Basis eines Arduinos

Zorn, Matthias

Einfluss variabler Stromprofile auf einen alkalischen Elektrolyseur

Unsere Mitarbeiter | Our Staff Members



Mitarbeiter | Staff Members

Name	Telefon	E-Mail	Arbeitsgebiet
	0711/685-	@ipv.uni-stuttgart.de	
Lydia Beisel	67169	lydia.beisel	Halbleitertechnologie Gruppenleiter
Peter Birke	67180	peter.birke	Elektr. Energiespeichersysteme
Christoph Bolsinger	67181	christoph.bolsinger	Elektr. Energiespeichersysteme
Susana Fernandez	67231	susana.fernandez-robledo	Industrielle Solarzellen
Mohamed Hassan	67163	mohamed.hassan	Laserprozesse
Fabian Heim	67245	fabian.heim	Elektr. Energiespeichersysteme
Freymut Hilscher	67141	freymut.hilscher	Verwaltung
Irmy Kerschbaum	67158	irmgard.kerschbaum	Verwaltung
Felix Kleinheinz	67184	felix.kleinheinz	Elektr. Energiespeichersysteme
Jürgen Köhler	67159	juergen.koehler	Gruppenleiter Laserprozesse
Pascal Kölblin	67179	pascal.koelblin	Sensorik
Timo Kropp	67246	timo.kropp	Sensorik

7 Mitarbeiter | Staff Members

Name	Telefon	E-Mail	Arbeitsgebiet
	0711- 685-	@ipv.uni- stuttgart.de	
Patrick Lill	67171	patrick.lill	Laserprozesse
Hendrik Moldenhauer	67142	hendrik. moldenhauer	Halbleiter- technologie
Sanaz Momeni	67183	sanaz. momeni	Elektr. Energiespei- chersysteme
Samer Mourad	67161	samer. mourad	Industrielle Solar- zellen
Daniel Müller	69214	daniel. mueller	Elektr. Energiespei- chersysteme
Jessica Nover	69213	jessica. nover	Industrielle Solar- zellen
Kathrin Ohmer	60889	kathrin. ohmer	Industrielle Solar- zellen
Sabine Ost	67141	sabine.ost	Verwaltung
Stephan Renninger	67181	stephan. renninger	Elektr. Energiespei- chersysteme
Alexander Ridder	67178	alexander. ridder	Elektr. Energiespei- chersysteme
Anton Riß	67214	anton.riss	Werkstatt
Matteo Schiliró	67198	matteo. schiliró	Industrielle Solar- zellen
Alexander Schmid	69223	alexander. schmid	Elektr. Energiespei- chersysteme
Markus Schubert	67145	markus. schubert	Gruppenleiter Sensorik

7 Mitarbeiter | Staff Members

Name	Telefon	E-Mail	Arbeitsgebiet
	0711- 685-	@ipv.uni- stuttgart.de	
Katja Schweiger	67200	katja. schweiger	Halbleitertechnologie
Johannes Siegel	60890	johannes. siegel	Sensorik
Jan Singer	69217	jan.singer	Elektr. Energiespei- chersysteme
Friedrich Speckmann	67182	friedrich. speckmann	Elektr. Energiespei- chersysteme
Marco Ströbel	69216	marco. stroebel	Elektr. Energiespei- chersysteme
Jürgen H. Werner	67140	juergen. werner	Institutsleiter
Evariste Pasky Wete	69218	evariste- pasky. wete	Industrielle Solar- zellen
Birgitt Winter	67162	birgitt. winter	Gruppenleiterin Halbleiter- technologie
Renate Zapf- Gottwick	69225	renate. zapf-gottwick	Gruppenleiterin Industrielle Solar- zellen

Mitarbeiter, ausgeschieden | Staff Members, departed

Leo Bauer

Kai Carstens

Morris Dahlinger

Erik Hoffmann

Tim Holch

Simon Huber

Sabrina Lang

Brigitte Lutz

Christian Sämann

Sabine Schreiber

Osama Tobail

Gäste & ausländische Stipendiaten | Guests

Mayunk Kulkarni

Manipal Institute of Technology, Manipal University /
Indien

Mohamed Hassan

Faculty of Engineering, Cairo University / Ägypten

Joshua Akuffo

Kwame Nkrumah University of Science and Technology,
Kumasi / Ghana

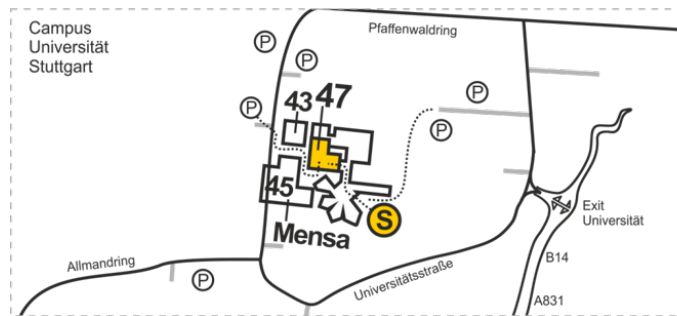
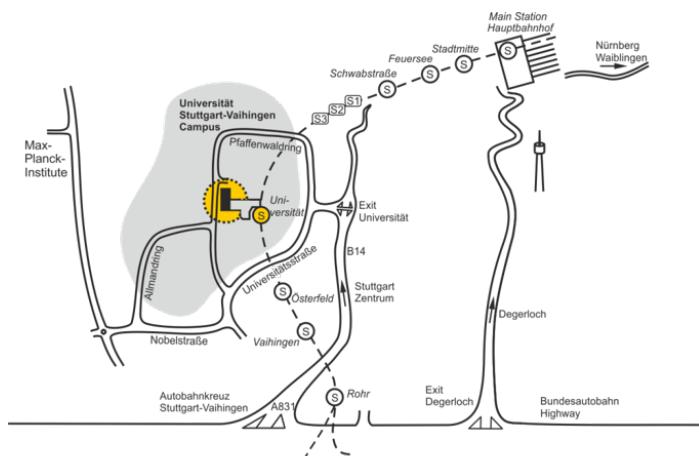
Qusay Twfeek Hassan

AGH University of Science and Technology, Krakow / Polen

Débora Cardoso Silveira

Universidade Federal de Minas Gerais, Belo Horizonte /
Brasilien

8 Lageplan | Location Map



Jahresbericht 2017 | 2018 des Instituts für Photovoltaik